

Effect of fine particles on the hydraulic behavior of interlayer soil in railway substructure

Trong Vinh Duong, Yu-Jun Cui, Anh Minh A.M. Tang, Jean Claude Dupla, Nicolas Calon

▶ **To cite this version:**

Trong Vinh Duong, Yu-Jun Cui, Anh Minh A.M. Tang, Jean Claude Dupla, Nicolas Calon. Effect of fine particles on the hydraulic behavior of interlayer soil in railway substructure. Canadian Geotechnical Journal, 2014, 51 (7), pp.735-746. 10.1139/cgj-2013-0170 . hal-01111160

HAL Id: hal-01111160
https://enpc.hal.science/hal-01111160

Submitted on 25 Apr 2018

HAL is a multi-disciplinary open access archive for the deposit and dissemination of scientific research documents, whether they are published or not. The documents may come from teaching and research institutions in France or abroad, or from public or private research centers.

L'archive ouverte pluridisciplinaire **HAL**, est destinée au dépôt et à la diffusion de documents scientifiques de niveau recherche, publiés ou non, émanant des établissements d'enseignement et de recherche français ou étrangers, des laboratoires publics ou privés.

Effect of fine particles on the hydraulic behavior of interlayer soil in railway substructure

Trong Vinh DUONG[1], Yu-Jun CUI[1], Anh Minh TANG[1], Jean-Claude DUPLA[1], Nicolas CALON[2]

[1] *Ecole des Ponts Paris Tech (ENPC), Laboratoire Navier/CERMES*

[2] *French Railway Company (SNCF)*

Corresponding author:

Prof. Yu-Jun CUI

Ecole des Ponts ParisTech

6-8 av. Blaise Pascal, Cité Descartes, Champs-sur-Marne

F-77455 MARNE LA VALLEE - France

Telephone : +33 1 64 15 35 50

Fax : +33 1 64 15 35 62

E-mail : yujun.cui@enpc.fr

Abstract:

The ancient railway substructure in France was built by emplacing ballast directly on sub-grade. Over years of operation, the inter-penetration of ballast and sub-grade created a soil layer between them. Under different conditions, this naturally formed layer, namely interlayer, can contain different quantities of fine particles, becoming more or less sensitive to changes in water content. As the water content changes are governed by the hydraulic behavior of interlayer soil, assessing the influence of fine particles content on the hydraulic behavior of interlayer soil is important. To this end, the hydraulic behavior of an interlayer soil taken from Sénissiat (near Lyon, France) was investigated using two infiltration columns, a large-scale column equipped with tensiometers and TDR for suction and volumetric water content measurements, respectively, and a smaller column equipped with high capacity tensiometers only. Different fines contents were considered and wetting-drying cycles were applied to the soil specimens. The hydraulic conductivity was determined by applying the instantaneous profile method. The results obtained showed that i) hysteresis exists for both the soil water retention curve and the hydraulic conductivity changes with suction; ii) the effect of wetting-drying cycles is insignificant; iii) adding 10% of fine particles to the natural interlayer soil changes the soil water retention curve but does not induce significant changes in hydraulic conductivity; iv) the hydraulic conductivity of interlayer soil with 10% of fine particles added is close to that of soil sieved at 2 mm, suggesting that the hydraulic conductivity of interlayer soil is mainly governed by fine particles through suction effect.

Keywords: railway substructure; interlayer soil; fines content; instantaneous profiles method; hydraulic conductivity.

Introduction

Many railway lines over the world have been in operation for more than one hundred years. In France, the ancient lines represent 94% of the whole railway network. As opposed to the new lines, the ancient ones were constructed by direct installation of ballast onto sub-grade without any separation layer. Over years of operation and with the increasing traffic, load, and speed of train, there are more and more problems related to the stability, loss of strength of substructure. A number of studies have been conducted to assess the state of substructure and to develop adequate maintenance methods (Trinh 2011; Duong et al. 2013; Cui et al. 2013). It was found that one of the particularities of ancient substructure is the presence of a soil layer namely interlayer that has been created mainly by interpenetration of ballast and fine particles of sub-grade.

In France, it has been decided recently to renew the ancient railway network. During the renewal, the interlayer will be kept as part of the substructure thanks to its high mechanical resistance related to its high dry unit mass (2.4 Mg/m^3 at the Sénissiat site, according to Trinh et al. 2011) reached by natural dynamic compaction corresponding to the circulation of trains. However, the mechanical behavior of interlayer soil can show a large variability, depending on the proportion of fine particles contained in it. A number of studies (Babic et al. 2000; Pedro 2004; Naeini and Baziar 2004; Kim et al. 2005; Verdugo and Hoz 2007; Cabalar 2008; Seif El Dine et al. 2010; Ebrahimi 2011; Anbazhagan et al. 2011; Trinh et al. 2012) showed that the mechanical behavior of soil containing a large proportion of fines is strongly influenced by the water content. As the water content changes are governed by the hydraulic behavior of soil, it appears important to assess the influence of fine particles content on the hydraulic behavior of interlayer soil.

Moreover, in field conditions, the interlayer soil normally undergoes the effect of wetting/drying cycles related to climatic changes. These wetting/drying cycles may induce changes in soil micro-structure, thereby changing the soil hydraulic properties. Therefore, it appears also important to investigate the effect of wetting/drying cycles on the hydraulic conductivity.

To the authors' knowledge, the effects of fines content and wetting/drying cycles on the unsaturated interlayer soil have not been investigated yet. In the present work, laboratory tests were performed using a large-scale infiltration column (300 mm in diameter) and a small-scale infiltration column (50 mm in diameter), and the instantaneous profile method was used to determine the hydraulic conductivity of soil. Both wetting and drying paths were performed and different fines contents were considered: natural interlayer soil (ITL_0), natural interlayer soil with 10% of sub-grade added (ITL_{10}), fine-grained soil prepared by passing ITL_{10} through a 2 mm sieve (*Fines*). The results enable the assessment of the effects of fine particles and wetting/drying cycles.

Materials studied

The soils (both the interlayer soil and sub-grade) were taken from the railway site Sénissiat (North-West of Lyon, France). Mineralogy analysis reveals that the interlayer soil is a mixture of materials that come from the construction and maintenance (broken stones, gravel, sand, etc) of tracks, the aging process of track components and the sub-grade. It also showed that the fine particles in the interlayer soil mainly come from the sub-grade. The main geotechnical properties of interlayer soil and sub-grade are presented in Table 1. The results show that the sub-grade is high-plasticity silt. More details about the characterization of the interlayer soil can be found in Trinh et al. (2011).

In order to study the effect of fines contents on the hydraulic behavior of interlayer soil, a quantity of sub-grade representing 10% of interlayer soil by dry mass was added into the interlayer soil to form a soil with a higher content of fines: ITL_{10}. The grain size distribution curves of the natural interlayer soil (ITL_0) and ITL_{10} are presented in Fig. 1.

It is worth noting that the migration of fines into ballast is recognized as one of the mechanisms for fouled ballast (Ayres 1986; Selig and Waters 1994; Alobaidi and Hoare 1996; 1998; Ghaotara et al. 2006; Mayoraz et al. 2006; Huang et al. 2009; Giannakos 2010; Fortunato et al. 2010; Indraratna et al. 2011; Ebrahimi 2011; Sussmann and Chrismer 2012). Even though the interlayer soil studied here is different from the fouled ballast by nature, in order to compare with the classification of fouled ballast, two parameters for fouled ballast are adopted here: the fouling index *FI* (Selig and Water 1994) and the relative fouling ratio $R_{b\text{-}f}$ (Indraratna et al. 2011). *FI* is defined as:

[1] $$FI = P_4 + P_{200}$$

where P_4 and P_{200} are percentages of ballast passing through sieves N° 4 (4.75 mm) and N° 200 (0.075 mm), respectively.

$R_{b\text{-}f}$ is the weighted ratio of the dry mass of fouling particles M_f (passing through 9.5 mm sieve) to the dry mass of ballast M_b (particles retained in 9.5 mm sieve):

[2] $$R_{b-f} = \frac{M_f \times \frac{G_{s-b}}{G_{s-f}}}{M_b} \times 100\%$$

where $G_{s\text{-}f}$, $G_{s\text{-}b}$ are specific densities of fouling particles and ballast, respectively.

The values of the two indexes for ITL_0 and ITL_{10} are presented in Table 2. According to the classification, both ITL_0 and ITL_{10} are "*highly fouled*". Because ITL_{10} is classified in the highest category of fouling, it was decided to not adding more fine particles to the interlayer soil.

To better evaluate the effect of fines on the hydraulic behavior of interlayer soil, the hydraulic conductivity of pure fine particles was also determined. For this purpose, ITL_{10} was sieved at 2 mm to obtain the fine part (namely *Fines*). The grain size distribution curve of *Fines* is also presented in Fig. 1.

Experimental methods

The interlayer soil was tested in a large-scale infiltration column (Fig. 2). The column (300 mm in diameter and 600 mm in height) is equipped with five water content sensors (TDR1 to TDR5) and five tensiometers for measuring pore-water pressure (T1 to T5) arranged at various elevations along the column (h = 100, 200, 300, 400 and 500 mm from the bottom of the soil specimen). The working pressure range of the tensiometers is from 100 kPa to -85 kPa. The accuracy of the TDR used is ± 2% and that of the tensiometer is ± 0.5 kPa. At each instrumented height, as the area occupied by the sensors is just 6.8% of the total apparatus section area, the influence of the sensors installation on water transfer is expected to be insignificant.

For the ITL_{10} specimen preparation, water and fine particles were added to the dry natural interlayer soil to reach the target water content and fine particles content, and a large mixer was used to homogenize the material. For the ITL_0 specimen preparation, only desired quantity of water was added to the dry natural interlayer soil. After mixing, the wet materials were stored in hermetic containers for at least 24 h for moisture homogenization. Soil compaction was conducted using a vibrating hammer in six layers of 0.10 m each at a dry unit mass of 2.01

128 Mg/m^3. The soil for each layer has a same composition as that of the whole sample. Big particles
129 and fine particles were rearranged before the compaction in order to ensure the sample
130 homogenization. Prior to the compaction of the subsequent layer, a TDR probe and a metal rod of
131 25 mm diameter were placed on the compacted layer.

132 Once the soil specimen was prepared, water was injected from the bottom and it flowed
133 out from the outlet after about half an hour. After saturation of the sample, the metal rods were
134 removed and the tensiometers were installed. This protocol was adopted to avoid damaging the
135 tensiometers during the compaction and also any cavitation due to possible high suction in the
136 column. More details about the large-scale infiltration column can be found in Duong et al.
137 (2013).

138 The TDR is an indirect measurement method and several authors reported that the
139 calibration curve depends on the soil texture, unit mass, mineralogy, fines content and particle
140 size (Jacobsen and Schjønning 1993; Stolte et al. 1994; Côté and Roy 1998; Gong et al. 2003;
141 Schneider and Fratta 2009). It is therefore necessary to determine the specific calibration curve
142 for each soil studied. For the natural interlayer soil (ITL_0), a relationship between volumetric
143 water content (θ) and the dielectric constant K_a was established by Duong et al. (2013). As the
144 soil composition in ITL_{10} is different from ITL_0, another relationship was needed. This was
145 determined separately with a lower specimen of 200 mm at the same unit mass in the same
146 column. One TDR sensor was placed in the middle of the sample. Water was added on the
147 surface of the soil specimen to achieve the desired water content. Once the TDR gave a steady
148 response (after about 8 hours), the water content was considered as being uniform within the
149 sample and the value of dielectric constant K_a was recorded. This operation was repeated until
150 the specimen reached full saturation (with 1 cm water on the soil surface). All the TDR sensors

were calibrated in the same fashion. The results obtained on the five sensors are similar. Fig. 3 presents the calibration curve of TDR for ITL_{10} along with the fitting calibration curve for ITL_0 presented in Duong et al. (2013) at the same dry unit mass (2.01 Mg/m^3). It can be observed that the curve for ITL_0 lies below the curve for ITL_{10}, indicating a clear effect of soil texture. The following equation (based on the model of Topp et al. 1980) was used to fit the experimental data for ITL_{10}:

[3] $$\theta = -4.16 \times 10^{-5} \times K_a^3 + 2.11 \times 10^{-3} \times K_a^2 - 2.36 \times 10^{-2} \times K_a + 0.17$$

The infiltration tests were conducted in two wetting/drying cycles. After installation of the tensiometers, the saturation of soil column was completed (Saturation 1). This wetting stage was followed by a draining stage (Drainage 1). Water was allowed to drain out through the bottom valves by keeping a constant water level at the bottom of soil sample using an external water source. The first wetting/drying cycle finished by a stage of evaporation (Evaporation 1) where the top cover of the column was removed to allow soil water evaporation. A fan was used to accelerate the evaporation process. The evaporation stage ended when the suction value indicated by tensiometer T5 (h = 500 mm) was about 60 kPa (higher suction would lead to cavitation). A second wetting-drying cycle was applied following the same procedure (Saturation 2, Drainage 2 and Evaporation 2). Before the second drainage, the hydraulic conductivity in saturated state was also measured by applying a constant water head of 0.61 m. The hydraulic gradient was 1. According to the Tennakoon et al. (2012), hydraulic gradient smaller than 4 can be considered as low enough to ensure the Darcy's law. Note that the experimental procedure with saturation from the bottom and evaporation from the top is also recommended in ASTM standard (ASTM 2010). During the measurement of hydraulic conductivity under saturated condition, the volume of water injected increased linearly with a rate of about 50 cm^3 per minute.

The unsaturated hydraulic conductivity of *Fines* was determined using a small-scale infiltration column of 50 mm in diameter and 200 mm in height (Munoz et al. 2008). Its schematic view is shown in Fig. 4. Suction measurements were performed by four high-capacity tensiometers (Cui et al. 2008) installed at 40, 80, 120 and 160 mm height from the base of the sample. The accuracy of this tensiometer is ± 1 kPa. The soil was statically compacted in the column in four layers of 50 mm each. Once the compaction was completed, the tensiometers were installed. In order to ensure a good contact between the soil sample and the tensiometers, a paste of sub-grade was applied on the surface of the ceramic of tensiometers.

The dry unit mass and water content of *Fines* were taken equal to those of fine particles contained in the sample of interlayer soil. Using the illustration shown in Fig. 5, these two parameters can be calculated as follows:

[4] $$\rho_{d,f} = \frac{M_{s,f}}{V_f} = \frac{M_s - M_{s,b}}{V - V_{s,b}} = \frac{(1-m)\rho_d V}{V - \frac{m}{\rho_{s,b}}\rho_d V} = \frac{(1-m)\rho_d \rho_{s,b}}{\rho_{s,b} - m\rho_d}$$

[5] $$w_f = \frac{M_w}{M_{s,f}} = \frac{M_s w}{M_s - M_{s,b}} = \frac{w}{1-m}$$

where M, M_w, M_s are the total mass, mass of water and mass of solid particles, respectively; V, V_w, V_s are the total volume, volume of water and volume of solid particles respectively; ρ_d, ρ_s are the dry unit mass of the specimen and unit mass of solid particles, respectively; the subscripts *f* and *b* stand for particle smaller and larger than 2 mm, respectively; m is the percentage of particles larger than 2 mm.

Based on the grain size distribution curve, a value $m = 0.67$ was determined. From Eqs (2) and (3), a value of 1.33 Mg/m^3 was obtained for the dry unit mass of *Fines*.

194 The test procedure followed for the small-scale infiltration column was akin to that for the
195 large-scale one. After the suction stabilization, the sample was saturated from the bottom
196 (Saturation 1). After completion of saturation, an external water source was connected to the
197 bottom in order to ensure a constant water level after the drainage. The top cover was then
198 removed allowing water evaporation from the soil surface (Evaporation 1). When suction at 160
199 mm reached about 400 kPa, Evaporation 1 was stopped to avoid cavitation of the tensiometers. A
200 second wetting-drying cycle was applied by following the same procedure as in the first cycle
201 (Saturation 2 and Evaporation 2).

202 Unlike the large-scale column where both suction and water content were monitored, the
203 small-scale column has only suction monitored. To obtain the water content changes during
204 infiltration, the soil-water retention curve (SWRC) was needed. The water retention curve (WRC)
205 of compacted *Fines* was determined separately using the device presented in Fig. 6. The soil was
206 first compacted inside an oedometer cell (the dimensions of the soil specimen are 50 mm in
207 diameter and 20 mm in height). The suction of the specimen was monitored by a high-capacity
208 tensiometer fixed at the bottom of the cell. A light aluminum piston of 50 mm diameter was
209 placed on the specimen to ensure the good contact between soil and tensiometer. The piston
210 induced a vertical stress of 1.8 kPa and its influence was believed to be negligible. For the
211 monitoring of soil water content, the whole system was placed on a balance having an accuracy
212 of ±0.01 g. The mass change indicated the quantity of water added or evaporated. More details
213 about this cell can be found in Le et al. (2011) and Munoz-Castelblanco et al. (2012). Wetting
214 was conducted by adding a small quantity of water on the upper face of the sample, while drying
215 was conducted by allowing soil water evaporation from the upper surface without the piston on it.
216 Once the desired water content was reached, the piston was put on the soil surface and the final
217 suction was recorded. This method was also discussed by Cunningham et al. (2003); Toker et al.

(2004); Loucenço (2008); Loucenço et al. (2011); Toll et al. (2012) and Munoz-Castelblanco et al. (2012).

For the large-scale column, both suction and water content profiles were obtained directly. For the small-scale column, the suction profiles were obtained directly while the water content profiles were determined through the SWRC. The instantaneous profile method (Daniel 1982; Delage and Cui 2001; Bruckler et al. 2002; Cui et al. 2008; Ye et al. 2009) was then applied for the determination of hydraulic conductivity for each soil. Note that this method is based on the generalized Darcy's law. The hydraulic gradient is determined by considering the slope of suction isochrones and the water volume passing through a given section between times t and $t+dt$ is used for calculating the water flux.

Experimental results

The results of ITL_0 were presented in Duong et al. (2013). Here only the results of ITL_{10} and *Fines* are presented in detail, and the results of ITL_0 are only used for comparison.

Fig. 7 presents changes in pore water pressure and volumetric water content versus time during Drainage 1 and Evaporation 1 for ITL_{10}. From the saturated state where the volumetric water content reached 22-25%, water drained out through the bottom valves and subsequently the volumetric water content decreased to 15 – 17% at the end of the draining stage for all the TDR sensors except that at h = 200 mm (Fig. 7b). At this moment, the pore water pressure was in the range from 0 to -4 kPa (Fig. 7a). Drainage 1 finished after more than 1 day. During Evaporation 1, the pore water pressure given by the tensiometer at h = 500 mm decreased quickly while small changes were observed at other levels (Fig. 7a). This is consistent with the values of volumetric

239 water content: the value at h = 500 m decreased significantly since the beginning of Evaporation
240 1 while those at other levels show slight changes (Fig. 7b).

241 During Saturation 2, the external water source was set at a level applying a water pressure
242 of 6.1 kPa to the bottom of sample. The results obtained show that less than one hour was needed
243 to re-saturate the soil specimen (Fig. 8). The changes were not significant for T1 to T4 (small
244 suction value), while those of T5 at h = 500 mm are quite significant (Fig. 8a). Furthermore, the
245 suction changes in Fig. 8a are consistent with those of volumetric water content in Fig. 8b. At the
246 end of this stage when the pore water pressure became positive at all levels, the 5 tensiometers
247 indicated the values corresponding to the water head at each level (5.5 kPa, 4.5 kPa, 3.5 kPa, 2.0
248 kPa and 1.0 kPa for T1 to T5, respectively). The volumetric water content also reached the values
249 of near saturated state (corresponding to the degree of saturations ranging from 87.5% to 100%).

250 The results obtained during Drainage 2 and Evaporation 2 are presented in Fig. 9. During
251 the first two days, water inside the column was connected to the outside water source having a
252 level decreased in steps of 50 mm from h = 550 to 50 mm in order to verify the response of the
253 sensors. Each step was kept for 1 hour. At the end of Drainage 2, the outside water source was set
254 at h = 50 mm and Evaporation 2 started. During the drainage, the volumetric water content
255 decreased quickly while the changes of suction were much slower. As during Evaporation 1, the
256 pore water pressure and the volumetric water content values at h = 500 mm decreased
257 significantly while the others remained almost constant. Once again, the changes of suction and
258 volumetric water content are consistent for different levels: the closer to the evaporation surface,
259 the higher the suction (Fig. 9a) and the smaller the volumetric water content (Fig. 9b) (except for
260 h = 200 mm).

The inconsistent data given by the TDR sensor at h = 200 mm (see Fig. 7, Fig. 8, Fig. 9) is related to the deficiency of this sensor. Indeed, some additional calibrations were conducted after the test, and the results showed some inertia of this TDR sensor: in the full range from 0 to 100%, no difference with other sensors was observed; however, in a limited range, a clear difference was identified. Thereby, the results by this sensor were not considered in further analysis.

The data of suction and volumetric water content recorded allowed the WRC of the interlayer soil to be determined. The results are presented in Fig. 10 with three paths corresponding to Drainage 1-Evaporation 1 (Drying 1), Saturation 2 (Wetting 2) and Drainage 1-Evaporation 2 (Drying 2). It can be observed that the results of two drying processes are close. In contrast, the result of wetting path lies above. Note that because the minimum recording interval of TDR was every minute and the wetting process took place very quickly; there are less data for the wetting path. The model of van Genuchten (1980) was used to fit the experimental data with the parameters presented in Table 3.

The hydraulic conductivity versus suction is presented in Fig. 11, including the hydraulic conductivity measured at saturated state, equal to 1.67×10^{-5} m/s. It can be seen that the results for the two drying paths are similar, suggesting negligible microstructure changes. For the wetting path, all results lie above those of the drying paths, illustrating a clear phenomenon of hysteresis. The models of van Genuchten (1980) and Brooks-Corey (Brooks and Corey 1964; Stankovich and Lockington 1995) were used for fitting the data of both drying and wetting paths using the least squares method (see Fig. 11). The parameters determined are presented in Table 4 .

Fig. 12 presents the comparison between the WRC of ITL_0 and ITL_{10} for the drying path (the parameters of van Genuchten's model (1980) used for fitting the experimental data are

284 presented in Table 3). Note that for clarity, the scattered data at low suction are not included. The
285 WRC of ITL_0 is beneath the WRC of ITL_{10}, suggesting that at a given suction, ITL_{10} has a higher
286 water content than ITL_0. This appears normal because with the same dry unit mass, the higher the
287 fines content, the higher the retention capacity.

288 The comparison of hydraulic conductivity between ITL_0 and ITL_{10} is presented in Fig. 13.
289 In the saturated state, the two soils have almost the same value: 1.67×10^{-5} m/s for ITL_{10} and
290 1.75×10^{-5} m/s for ITL_0. Both values are lower than the critical value proposed by Selig and
291 Waters (1994) for the railway substructures. In unsaturated state, even the data are scattered for
292 the two soils, an identical trend can be identified: the hydraulic conductivity is decreasing with
293 the increase of suction. Moreover, the average value for ITL_{10} is slightly higher than that for ITL_0,
294 suggesting a slightly greater hydraulic conductivity for ITL_{10}. On the whole, the difference
295 between the hydraulic conductivity results of two soils is less evident than the difference between
296 the SWRC results.

297 The results obtained from the small-scale infiltration test on *Fines* are shown in Fig. 14 to
298 Fig. 18. After installation of the tensiometers, a period of 18 hours was needed to reach the
299 suction equilibrium at 70 – 83 kPa (Fig. 14). This difference in final suctions at different levels
300 was mainly related to the soil heterogeneity. The corresponding degree of saturation was 43%.
301 From this initial state, the soil was first re-saturated by injecting water from the bottom with a
302 constant water head of 0.7 kPa. The suction at the lowest level changed first, followed by the
303 suctions at higher levels (Fig. 15). Ten minutes after the water injection, water appeared on the
304 upper surface and suctions at all level reached zero, indicating the full saturation of the soil
305 specimen.

306 After Saturation 1, water was drained out to an outside water source and the water level
307 was maintained at h = 0. Afterwards, Evaporation 1 took place. The results obtained are shown in
308 Fig. 16. Fifteen hours later, the pore water pressure measured at h = 160 mm (40 mm below the
309 soil surface) started to decrease and reached -300 kPa at 57 hours. The changes in water pressures
310 measured by other tensiometers were less significant.

311 Saturation 2 took place right after Evaporation 1. The results obtained during this second
312 wetting stage are shown in Fig. 17. Less than 2 minutes was required for the pore water pressure
313 at h = 160 mm to come back from -300 kPa to about 0. The results obtained during the
314 subsequent drying are shown in Fig. 18 (Evaporation 2). As in the case of Evaporation 1, after 80
315 hours, the pore water pressure at h = 160 mm decreased to - 365 kPa while those at other levels
316 did not change significantly.

317 The results from the test in the tensiometer-equipped oedometer are shown in Fig. 19. Fig.
318 19a depicts the suction (negative pore water pressure given by the tesiometer) evolution after the
319 tensiometer installation. The suction increased and reached its stabilization value of 110 kPa after
320 17 hours. This corresponds to the initial state of the soil specimen (21.3 % volumetric water
321 content and 42.6 % degree of saturation). Water was then added into the specimen to follow the
322 wetting path. The variation of the first step of wetting is presented in Fig. 19b. About 35 minutes
323 was needed for suction stabilization. The volumetric water content in this step increased from
324 21.3% to 21.7%. This operation was repeated until the soil reached the near saturated state. Then
325 the drying steps started. Fig. 19c presents the suction stabilization during one drying step. An
326 equilibrium value of 79 kPa was reached after 320 minutes. This suction increase corresponded to
327 a decrease of volumetric water content from 22.2% to 21.6%.

328 The SWRC obtained for *Fines* is shown in Fig. 20. From its initial state, the soil specimen
329 was subjected to wetting up to 70% degree of saturation, followed by drying and finally a second
330 wetting till full saturation. It can be seen that the SWRC obtained during drying lies above that
331 during wetting. The maximum suction value was 390 kPa corresponding to a volumetric water
332 content of 18.9%; it was also close to the maximum suction value in the specimen during the
333 infiltration test, indicating the compatibility of the two tests.

334 This SWRC determined was then used to calculate the changes of volumetric water
335 content in the small-scale infiltration column based on the suction changes presented in Fig. 15 to
336 Fig. 18. Either the drying or the wetting path was used depending on the path followed in the
337 infiltration test. As the second drying path of SWRC was not available, the first drying path was
338 used for calculating the volumetric water content during the second drying path in the infiltration
339 test. Then, based on the profiles of suction and water content, the hydraulic conductivity of
340 compacted *Fines* was calculated. The results are shown in Fig. 21, including the hydraulic
341 conductivity measured at saturated state by applying a constant water pressure of 0.7 kPa:
342 2.6×10^{-6} m/s. Albeit the large data scatter, a clear trend can be observed: as for the interlayer soil,
343 the hydraulic conductivity increased when the suction decreased.

344 It is worth noting that the results obtained for the two drying paths are quite similar. The
345 same conclusion can be drawn for the two wetting paths. The models of van Genuchten (1980)
346 and Brooks-Corey (Brooks and Corey 1964; Stankovich and Lockington 1995) were used to fit
347 the results (Fig. 21), and the parameters determined are presented in Table 4. Comparison
348 between the drying and wetting curves shows that for the 2 wetting/drying cycles, the wetting
349 curves lie always above the drying curves. It is opposed to the SWRC where the wetting curves
350 are normally beneath the drying ones. In addition, the curves of wetting path and drying path of

351 the 1st cycle are close to those corresponding to the 2nd cycle, suggesting no effect of
352 wetting/drying cycles on the hydraulic conductivity. The smallest value of hydraulic conductivity
353 identified is 6×10^{-12} m/s corresponding to a suction value of 242 kPa, while the highest one is
354 2.6×10^{-6} m/s corresponding to the saturated state.

355 Fig. 22 depicts the comparison of SWRC between ITL_{10} and *Fines* in the plane of degree
356 of saturation versus suction. The two curves start from almost the same point - around 97%
357 degree of saturation and 1.7 kPa suction. From 3 kPa suction, the WRC of ITL_{10} starts to separate
358 from the WRC of ITL_0. The two curves are parallel (for drying path) from 10 kPa suction. The
359 curves of ITL_{10} stop at 71 kPa while the curves of *Fines* stop at 389 kPa due to the different
360 capacities of the tensiometers used for the two soils. The gap between two curves is about 10% of
361 degree of saturation at the end of the curve for ITL_{10}.

362 In Fig. 23, the hydraulic conductivity of ITL_{10} and *Fines* is plotted versus suction. It can
363 be observed that the wetting and drying curves of the interlayer soil are quite close to those of
364 *Fines*, suggesting that the hydraulic conductivity of the interlayer soil is mainly governed by the
365 hydraulic conductivity of the fines contained in it. In other words, water transfer in the interlayer
366 soil takes place mainly through the network of pores between fine particles, coarse elements like
367 ballast behaving as inert materials. This is confirmed by the hydraulic conductivity values at
368 saturated state: similar values were identified - 1.67×10^{-5} m/s for ITL_{10} against 2.6×10^{-6} m/s for
369 *Fines*.

370 From a practical point of view, Fig. 23 shows that to determine the hydraulic conductivity
371 of interlayer soils, it is not necessary to use large-scale experimental devices to match the soil
372 grain size; smaller devices can be used to determine their hydraulic conductivity by testing the
373 fine particles only, provided that equivalent dry density is accounted for.

Discussions

Fig. 11 and Fig. 21 show the uncommon phenomenon of hystersis observed in hydraulic conductivity of ITL_{10} and *Fines*, respectively. The curve of wetting path lies above the curve of drying path. The same phenomenon was observed by Wayllace and Lu (2011). The following interpretations can be attempted.

Due to the different kinetic between the fast liquid transfer in wetting and the long vapor transfer in drying, the time needed for drying was much longer than that for wetting. This phenomenon was also reported by Toker et al. (2004) and discussed by Munoz-Castelblanco et al. (2012). A higher hydraulic conductivity can be expected in that case for wetting path.

In the present work, the calculation of hydraulic conductivity was performed based on the suction evolution given by tensiometers. Assuming that in the compacted soils, both macro-pores and micro-pores existed. During wetting, the macro-pores were filled with water more quickly than micro-pores. Moreover, in the micro-pores, there were always air bubbles preventing the total saturation. In contrast, during drying, all pores (micro and macro) participated in the evaporation process. As a result, when water filled the macro-pores, the tensiometers immediately gave the suction changes corresponding to the water flow through the macro-pores, even though the suction in micro-pores would be higher. On the contrary, when water evaporates during drying, the tensiometers gave the suction changes that involve both macro and micro-pores, in a much slower fashion. In other words, the suction measured by the tensiometers was probably under-estimated for wetting paths. Côté and Roy (1998) also reported that one re-saturating stage is not enough to fully saturate a soil sample because of the air bubbles trapped in micro-pores. This can also explain the uncommon hysteresis mentioned before.

Poulovassilis (1969) (cited by Mualem 1976) considered, in a qualitative way, the influence of capillary hysteresis on the hydraulic conductivity based on the concept of independent domain theory. He defined two mechanisms related to hysteresis: (i) water fills pores of larger opening radius in a wetting process than in drying one; (ii) the pores configuration and interconnection may be different for wetting and drying. As a result, the hydraulic conductivity in wetting may be different from that in drying for the same water content. The theory about the difference between the opening radius affecting wetting process and the opening radius affecting drying process is known as the effect of ink-bottle (Bertotti and Mayergoyz 2006; Naumov 2009). According to this theory, the pores affecting the wetting curve are larger than the pores affecting the drying curve. As a result, the water transfer is faster during wetting than during drying, implying a higher hydraulic conductivity in the case of wetting.

Conclusions

Infiltration tests were performed on the interlayer soil (ITL_0) and its derived soils - adding 10% of sub-grade to form ITL_{10} and sieving ITL_{10} at 2 mm to form *Fines*. Two wetting/drying cycles were applied for each test. The obtained results allowed the effect of fine particles on the water retention capacity and hydraulic conductivity of interlayer soil to be analyzed.

The effect of wetting/drying cycles on hydraulic conductivity was found negligible - the results of the first cycle are quite similar to those of the second cycle, suggesting an insignificant microstructure change by wetting/drying cycles.

Hysteresis exists for both the soil water retention curve and the hydraulic conductivity changes with suction. The wetting process was found to be much faster than the drying process, and the hydraulic conductivity during wetting is always higher than that during drying. This can

418 be explained by the effect of ink-bottle and the difference between the water transfer through the
419 network of macro-pores and micro-pores.

420 Adding 10% fine particles to the natural interlayer soil changes the soil water retention
421 curve but does not induce significant changes in hydraulic conductivity. In saturated state, the
422 hydraulic conductivity of natural interlayer soil is 1.75×10^{-5} m/s, while the value of the soil with
423 10% fines added is 1.67×10^{-6} m/s. In unsaturated state, even though the results are little scattered,
424 the results of ITL_{10} are within the variation range of the results of ITL_0. However, it is worth
425 noting that the mean value of ITL_{10} is slightly greater than that of ITL_0.

426 The water retention curves of ITL_{10} and *Fines* are different, illustrating an obvious effect
427 of soil texture. On the contrary, in terms of hydraulic conductivity including the values in
428 saturated state, a good agreement was identified between the results of two soils, regardless of the
429 drying or wetting paths. This suggests that water transfer in the interlayer soil takes place mainly
430 through the network of pores between fine particles, coarse elements like ballast behaving as inert
431 materials. From a practical point of view, this finding shows that to determine the hydraulic
432 conductivity of interlayer soils, a device as small as the small-scale infiltration cell can be
433 employed to determine the hydraulic conductivity of interlayer soil by testing the fine particles
434 only, provided that equivalent dry density is taken into account.

435

436 ## *Acknowledgements*

437 The present work is part of the project RUFEX (Re-use of ancient railway platforms and existing
438 foundations) funded by the French National Research Agency. The supports of French Railway
439 Company (SNCF) and Ecole des Ponts ParisTech are also gratefully acknowledged.

Reference

Alobaidi, I., and Hoare, D. 1996. The development of pore water pressure at the sub-grade-subbase interface of a highway pavement and its effect on pumping of fines. Geotextiles and geomembranes, **14**: 111-135.

Alobaidi, I., and Hoare, D. 1998. The role of geotextile reinforcement in the control of pumping at the sub-grade-subbase interface of highway pavements. Geosynthetics International, **5**(6): 619–636.

AFNOR. 2005. Identification and classification of soil- Part 2: Principles for a classification. NF EN ISO 14688.

Anbazhagan, P., Lijun, S., Buddhima, I., and Cholachat, R. 2011. Model track studies on fouled ballast using ground penetrating radar and multichannel analysis of surface wave. Journal of Applied Geophysics, **74**(4): 175–184.

ASTM 2010. Standard test method for measurement of hydraulic conductivity of unsaturated soils. D7664-10.

Ayres, D. 1986. Geotextiles or geomembranes in track? British railways' experience. Geotextiles and Geomembranes, **3**(2-3): 129–142.

Babic, B., Prager, A., and Rukavina, T. 2000. Effect of fine particles on some characteristics of granular base courses. Materials and Structures, **7**(33): 419-424.

Bertotti, G., and Mayergoyz, I. D. 2006. The science of hysteresis III. Academic Press

Brooks, R.H., and Corey, A.T., 1964. Hydraulic properties of porous media. Hydro. Paper No.3, Colorado State Univ., Fort Collins, Colo.

Bruckler, L. B., Angulo-Jaramillo, P., and Ruy, R. 2002. Testing an infiltration method for estimating soil hydraulic properties in the laboratory. Soil Science Society of America Journal, **66**: 384–395.

Cabalar, A. 2008. Effect of fines content on the behavior of mixed specimens of a sand. Electronic Journal of Geotechnical Engineering, **13**(D): 1-11.

Côté, J., and Roy, M. 1998. Conductivité hydraulique de matériaux de fondations de chaussées partiellement saturés (In French). Rapport de l'études et recherches en transports du Québec, 177p.

Cui, Y.J., Duong, T.V., Tang, A.M., Dupla, J.C., Calon, N., and Robinet, A. 2013. Investigation of the hydro-mechanical behaviour of fouled ballast. Journal of Zhejiang University-Science A (Applied Physics & Engineering), **14**(4): 244-255.

Cui, Y. J., Tang, A. M., Mantho, A., and Delaure, E. 2008. Monitoring field soil suction using a miniature tensiometer. Geotechnical Testing Journal, **31**(1) : 95-100.

Cui, Y. J., Tang, A. M., Loiseau, C., and Delage, P. 2008. Determining the unsaturated hydraulic conductivity of a compacted sand-bentonite mixture under constant-volume and free-swell conditions. Physics and Chemistry of the Earth, Parts A/B/C, 33: S462–S471.

Cunningham, M., Ridley, A., Dineen, K., and Burland, J. 2003. The mechanical behaviour of a reconstituted unsaturated silty clay. Géotechnique, **53** (2): 183-194.

Daniel, D. E. 1982. Measurement of hydraulic conductivity of unsaturated soils with thermocouple psychometers. Soil Science Society of American Journal, **46**(6): 1125–1129.

Delage, P., and Cui, Y. J. 2001. Comportement mécanique des sols non saturés. Article C302. Ed. Techniques Ingénieur.

Duong, T. V., Tang, A. M., Cui., Y. J., Trinh, V. N., and Calon, N. 2013. Development of a large-scale infiltration column for studying the hydraulic conductivity of unsaturated fouled ballast. Geotechnical Testing Journal, **36**(1): 55-63.

Ebrahimi, A. 2011. Behavior or fouled ballast. Railway Track and Structures, **107**(8): 25–31.

Fortunato, E., Pinelo, A., and Matos Fernandes, M. 2010. Characterization of the fouled ballast layer in the substructure of a 19th century railway track under renewal. Soils and Foundations, **50**(1): 55–62.

Ghataora, G., Burns, B., Burrow, M., and Evdorides, H. 2006. Development of an index test for assessing anti-pumping materials in railway track foundations. Proc.,First International Conference on Railway Foundaitons. 355–366.

Giannakos, K. 2010. Loads on track, ballast fouling, and life cycle under dynamic loading in railways. Journal of Transportation Engineering, **136**(12): 1075–1084.

Gong, Y., Cao, Q., and Sun, Z. 2003. The effects of soil bulk density, clay content and temperature on soil water content measurement using time-domain reflectometry. Hydrological Processes, **17**(18): 3601–3614.

Huang, H., Tutumluer, E., and Dombrow, W. 2009. Laboratory characterization of fouled railroad ballast behavior. Transportation Research Record: Journal of the Transportation Research Board, **2117**(1): 93–101.

Indraratna, B., Salim, W., and Rujikiatkamjorn, C. 2011. Advanced Rail Geotechnology - Ballasted Track. CRC Press.

Jacobsen, O. H., and Schjønning, P. 1993. A laboratory calibration of time domain reflectometry for soil water measurement including effects of bulk density and texture. Journal of Hydrology, **151**(2-4): 147–157.

506 Kim, D., Sagong, M., and Lee, Y. 2005. Effects of fine aggregate content on the mechanical
507 properties of the compacted decomposed granitic soils. Construction and Building Materials,
508 **19**(3): 189–196.

509 Le, T.T., Cui, Y.J., Muñoz, J.J., Delage, P., Tang, A.M., and Li; X.L. 2011. Studying the stress-
510 suction coupling in soils using an oedometer equipped with a high capacity tensiometer. Frontiers
511 of Architecture and Civil Engineering in China **5**(2): 160-170.

512 Lourenço, S. 2008. Suction measurements and water retention in unsaturated soils.
513 PhD dissertation, Durham University.

514 Lourenço, S., Gallipoli, D., Toll, D., Augarde, C., and Evans, F. 2011. A new procedure for the
515 determination of soil-water retention curves by continuous drying using high-suction
516 tensiometers. Canadian Geotechnical Journal, **48**(2): 327-335

517 Mayoraz, F., Vulliet, L., and Laloui, L. 2006. Attrition and particle breakage under monotonic
518 and cyclic loading. Comptes Rendus Mécanique, **334**(1): 1–7.

519 Mualem, Y. 1976. Hysteretical models for prediction of the hydraulic conductivity of unsaturated
520 porous media. Water Resources Research, **12**(6): 1248-1254.

521 Munoz, J. J., De Gennaro, V., and Delaure, E. 2008. Experimental determination of unsaturated
522 hydraulic conductivity in compacted silt. In Unsaturated soils: advances in geo-engineering:
523 proceedings of the 1st European Conference on Unsaturated Soils, E-UNSAT 2008, Durham,
524 United Kingdom, 2-4 July 2008, pp.123-127.

525 Munoz-Castelblanco, J. A., Pereira, J. M., Delage, P., and Cui, Y. J. 2012. The water retention
526 properties of a natural unsaturated loess from northern France. Géotechnique, **62**(2): 95-106.

527 Naumov, S. 2009. Hysteresis phenomenon in Mesoporous Materials. PhD Dissertation,
528 University of Leipzig.

529 Naeini, S., and Baziar, M. 2004. Effect of fines content on steady-state strength of mixed and
530 layered specimens of a sand. Soil Dynamics and Earthquake Engineering, **24**(3): 181–187.

531 Pedro, L. 2004. De l'étude du comportement mécanique de sols hétérogènes modèles à son
532 application au cas des sols naturels. PhD disertation, Ecole Nationale des Ponts et Chaussées,
533 France. (In French).

534 Poulovassilis, A. 1969. The effect of hysteresis of pore water on the hydraulic conductivity. Soil
535 Science, **20**: 52-56.

536 Schneider, J. M., and Fratta, D. 2009. Time-domain reflectometry - parametric study for the
537 evaluation of physical properties in soils. Canadian Geotechnical Journal, **46**(7): 753–767.

538 Selig, E. T., and Waters, J. M. 1994. Track geotechnology and substructure management.
539 Thomas Telford.

Seif El Dine, S., Dupla, J., Frank, R., Canou, J., and Kazan, Y. 2010. Mechanical characterization of matrix coarse-grained soils with a large-sized triaxial device. Canadian Geotechnical Journal, **47**(4): 425–438.

Stankovich J. M., and Lockington, D. A., 1995. Brooks-Corey and van Genuchten, soil-water-retention models. Journal of Irrigation and Drainage Engineering, 121(1): 1-7.

Stolte, J., Veerman, M ., Wosten, G. J., Freijer, J. H. M., Bouten, J. I ., Dirksen, W., Van Dam, C., and Van den Berg, J.C. 1994. Comparison of six methods to determine unsaturated soil hydraulic conductivity. Soil Science Society of America Journal, **58**(6): 1596-1603.

Sussmann, T. R., Ruel, M., and Christmer, S. 2012. Sources, influence, and criteria for ballast fouling condition assessment. Proc., 91st Annual Meeting of the Transportation Research Board. 11p.

Tennakoon, N., Indraratna, B., Rujikiatkamjorn, C., Nimbalkar, S., and Neville, T. 2012. The role of ballast-fouling characteristics on the drainage capacity of a rail substructure. Geotechnical Testing Journal, **35**(4): 1-12.

Toker, N., Germaine, J., Sjoblomt, K. and Culligan, P. 2004. A new technique for rapid measurement of continuous soil moisture characteristic curves. Géotechnique, **54**(3): 179-186.

Toll, D., Lourenço, S., and Mendes, J. 2012. Advances in suction measurements using high suction tensiometers. Engineering Geology. doi.org/10.1016/j.enggeo.2012.04.013.

Topp, G. C., Davis, J. L., and Annan, A. P. 1980. Electromagnetic determination of soil water content: measurements in coaxial transmission lines. Water Resource Research, (16): 574-582.

Trinh, V.N. 2011. Comportement hydromécanique des matériaux constitutifs de plateformes ferroviaires anciennes. (In French). PhD Dissertation, Ecole Nationales des Ponts et Chaussées - Université Paris – Est.

Trinh, V. N., Tang, A. M., Cui, Y. J., Canou, J., Dupla, J.C., Calon, N., Lambert, L., Robinet, A., and Schoen, O. 2011. Caractérisation des matériaux constitutifs de plate-forme ferroviaire ancienne. (In French). Revue Française de Géotechnique, (134-135): 65–74.

Trinh, V.N., Tang, A.M., Cui, Y.J., Dupla, J.C., Canou, J., Calon, N., Lambert, L., Robinet, A., and Schoen, O. 2012. Mechanical characterisation of the fouled ballast in ancient railway track substructure by large-scale triaxial tests. Soils and Foundations, **52**(3): 511-523.

van Genuchten, M.T. 1980. A closed-form equation for predicting the hydraulic conductivity of unsaturated soils. Soil Science Society of America Journal, **44**(5): 892–898.

Verdugo, R., and Hoz, K. 2007. Strength and stiffness of coarse granular soils. Solid Mechanics and Its Application, **146**(3): 243–252.

573 Wayllace, A., and Lu, N. 2011. A transient water release and imbibitions method for rapidly
574 measuring wetting and drying soil water retention and hydraulic conductivity functions.
575 Geotechnical Testing Journal, **35**(1): 1-15.

576 Ye, W. M., Cui, Y. J., Qian, L. X., and Chen, B. 2009. An experimental study of the water
577 transfer through compacted GMZ bentonite. Engineering Geology, **108**(3): 169– 176.

578

List of table

Table 1: Properties of the soil studied
Table 2: Fouling state of the interlayer soil
Table 3: Parameters of the van Genuchten's model (1980) for the soil water retention curves of interlayer soil
Table 4: Parameters of the van Genuchten's model and Brooks-Corey's model for the hydraulic conductivity of ITL_{10} and *Fines*

List of figures

Fig. 1: Grain size distribution curves of the interlayer soil (*ITL_0) and its derived ones* (*ITL_{10}* and *Fines*)
Fig. 2: Schematic view of the large-scale infiltration column
Fig. 3: Calibration curves of the TDRs used for the ITL_{10} and ITL_0 specimens
Fig. 4: Schematic view of the small-scale infiltration column
Fig. 5: Components of the unsaturated interlayer soil
Fig. 6: Device for determining the WRC of *Fines*
Fig. 7: Test on ITL_{10}: pore water pressure and volumetric water content evolutions during Drainage 1 and Evaporation 1
Fig. 8: Test on ITL_{10}: pore water pressure and volumetric water content evolutions in Saturation 2
Fig. 9: Test on ITL_{10}: pore water pressure and volumetric water content evolutions during Drainage 2 and Evaporation 2
Fig. 10: WRC of ITL_{10} with fitting curves using the van Genuchten's model (1980)
Fig. 11: Hydraulic conductivity of ITL_{10} obtained with drying-wetting cycles
Fig. 12: Comparison of SWRC between ITL_0 and ITL_{10}
Fig. 13: Comparison of hydraulic conductivity between ITL_0 and ITL_{10}
Fig. 14: Test on *Fines*: suction stabilization after the installation of tensiometers
Fig. 15: Test on *Fines*: suction evolutions during Saturation 1
Fig. 16: Test on *Fines*: suction evolutions during Evaporation 1
Fig. 17: Test on *Fines*: suction evolutions during Saturation 2
Fig. 18: Test on *Fines*: suction evolutions during Evaporation 2
Fig. 19: Stabilization of suction during the SWRC determination. (a) initial stabilization after tensiometer installation, (b) a wetting stage, (c) a drying stage
Fig. 20: WRC of *Fines*
Fig. 21: Hydraulic conductivity of *Fines*, obtained with drying/wetting cycles
Fig. 22: Comparison of SWRC between ITL_{10} and *Fines*
Fig. 23: Comparison of hydraulic conductivity between ITL_{10} and *Fines*

Table 1: Properties of the soil studied

Soil	Properties	Value
Interlayer soil (ITL_0)	ρ_s (particles smaller than 2 mm)	2.67 Mg/m^3
	ρ_s (particles larger than 2 mm)	2.68 Mg/m^3
	d_{10}	0.01 mm
	d_{30}	5 mm
	d_{60}	30 mm
	liquid limit w_L (smaller than 100 μm)	40.2%
	plasticity index I_p (smaller than 100 μm)	11.3%
Sub-grade (Fines to create ITL_{10})	*liquid limit* w_L	57.8%
	plasticity index I_p	24.1%

Table 2: Fouling state of the interlayer soil

	Fouling Index FI (-)	Relative ballast fouling ratio $R_{b\text{-}f}$ (%)	Fouling category
ITL_0	45	56	Highly fouled
ITL_{10}	59	72	Highly fouled

Table 3: Parameters of the van Genuchten's model (1980) for the soil water retention curves of interlayer soil

	Natural interlayer soil (ITL_0)	**Interlayer soil with 10% sub-soil added (ITL_{10})**		
Formula	**Drying**	**Drying 1**	**Wetting 2**	**Drying 2**
$\theta = \theta_r + \frac{\theta_s - \theta_r}{\left[1+(\alpha h)^n\right]^m}$	θ_s = 25 θ_r = 0 α = 4 n = 1.17 m = 0.15	θ_s = 25 θ_r = 10 α = 159.62 n = 1.24 m = 0.19	θ_s = 22.5 θ_r = 10 α = 0.19 n = 5.24 m = 0.81	θ_s = 25 θ_r = 10 α = 113.45 n = 1.25 m = 0.2

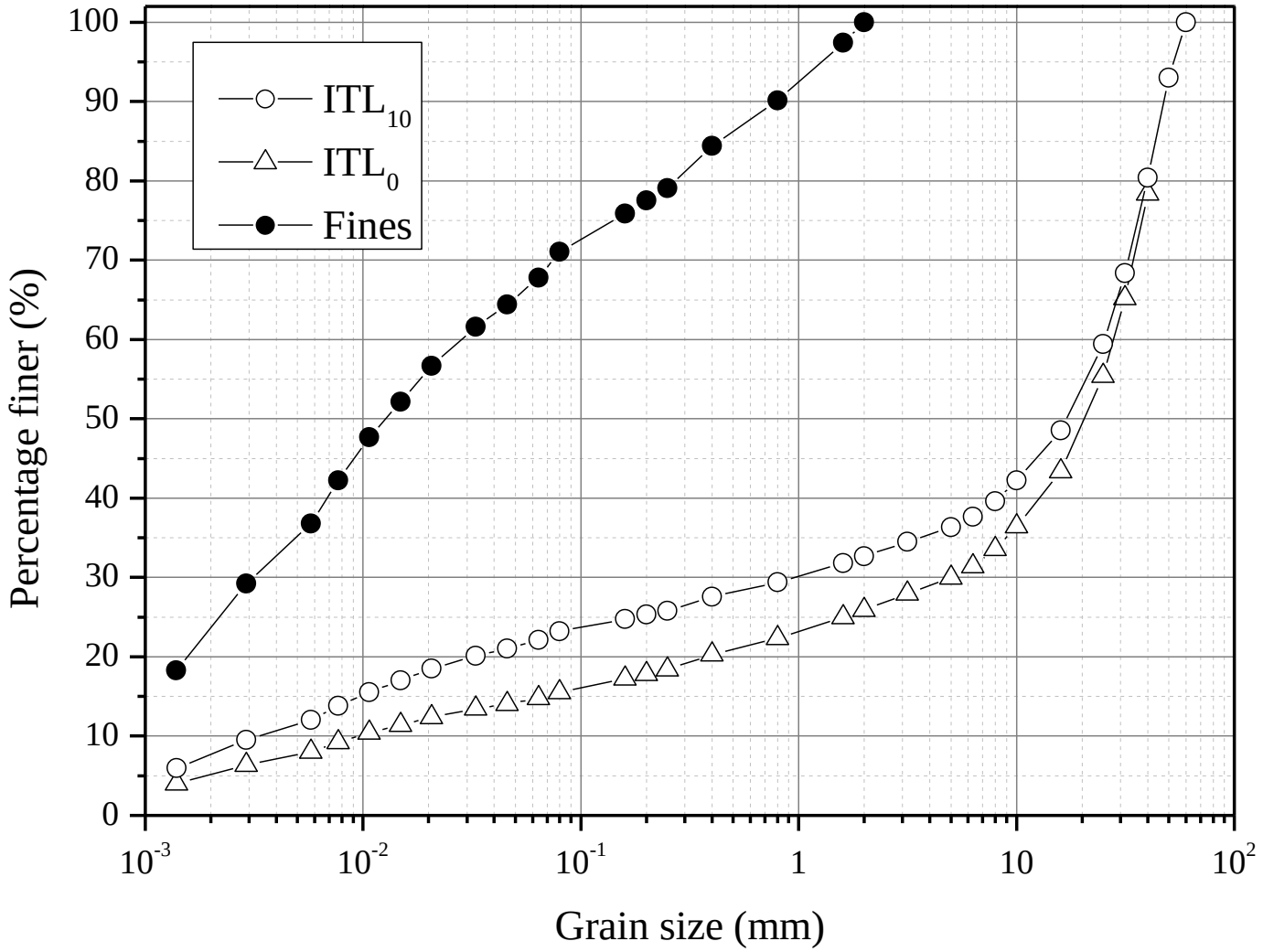
Notes: θ is volumetric water content (%); θ_s is the volumetric water content at saturated state (%); θ_r is the residual volumetric water content (%); h is hydraulic head in meter; α, n, m are the model's parameters

Table 4: Parameters of the van Genuchten's model and Brooks-Corey's model for the hydraulic conductivity of ITL_{10} and *Fines*

Model	Formula	Soil	Drying path	Wetting path
van Genuchten	$k = k_s \frac{1-(\alpha h)^{n-2}\left[1+(\alpha h)^n\right]^{-m}}{\left[1+(\alpha h)^n\right]^{2m}}$	ITL_{10}	α = 7.16 n = 2.12 m = 0.06	α = 0.5 n = 2.4 m = 0.17
		Fines	α = 2.1 n = 2.06	α = 0.25 n = 2.37

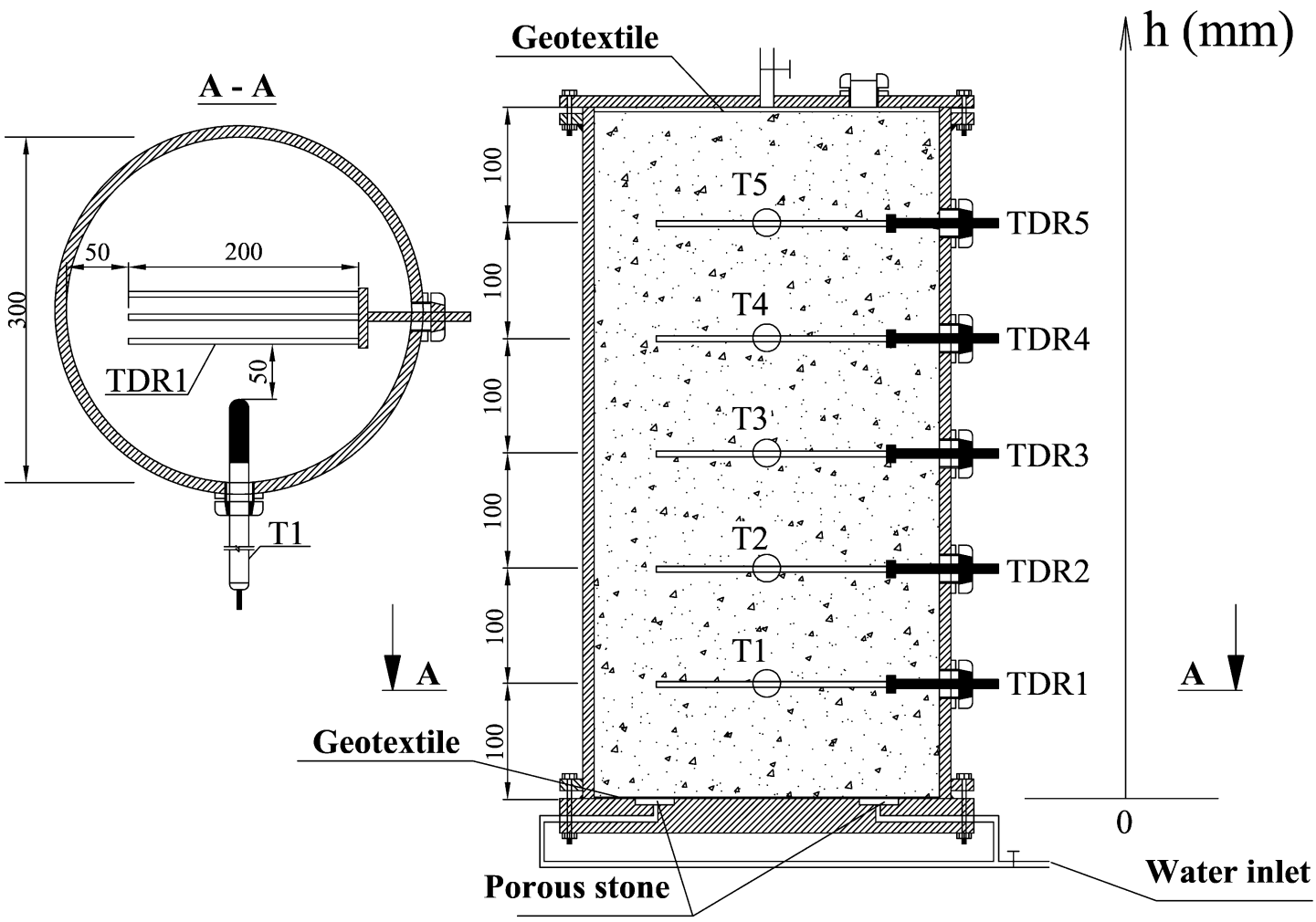
			m = 0.03	*m = 0.15*
		For the two soils	*α = 2.2* *n = 2.1* *m = 0.05*	*α = 0.3* *n = 2.7* *m = 0.16*
Brooks-Corey	$k = k_s \left(\frac{s_a}{s} \right)^{2+3\lambda}$	*ITL*$_{10}$	$s_a = 0.3$ $\lambda = 0.05$	$s_a = 4$ $\lambda = 0.1$
		Fines	$s_a = 0.7$ $\lambda = 0.01$	$s_a = 7$ $\lambda = 0.01$
		For the two soils	$s_a = 0.74$ $\lambda = 0.03$	$s_a = 5.4$ $\lambda = 0.02$

627 *Notes: k* is the hydraulic conductivity; k_s is the hydraulic conductivity in saturated state; *h* is
628 hydraulic head in meter; *s* is the suction (kPa); s_a is the air-entry value (kPa); λ, α, *n, m* are
629 parameters of the models.



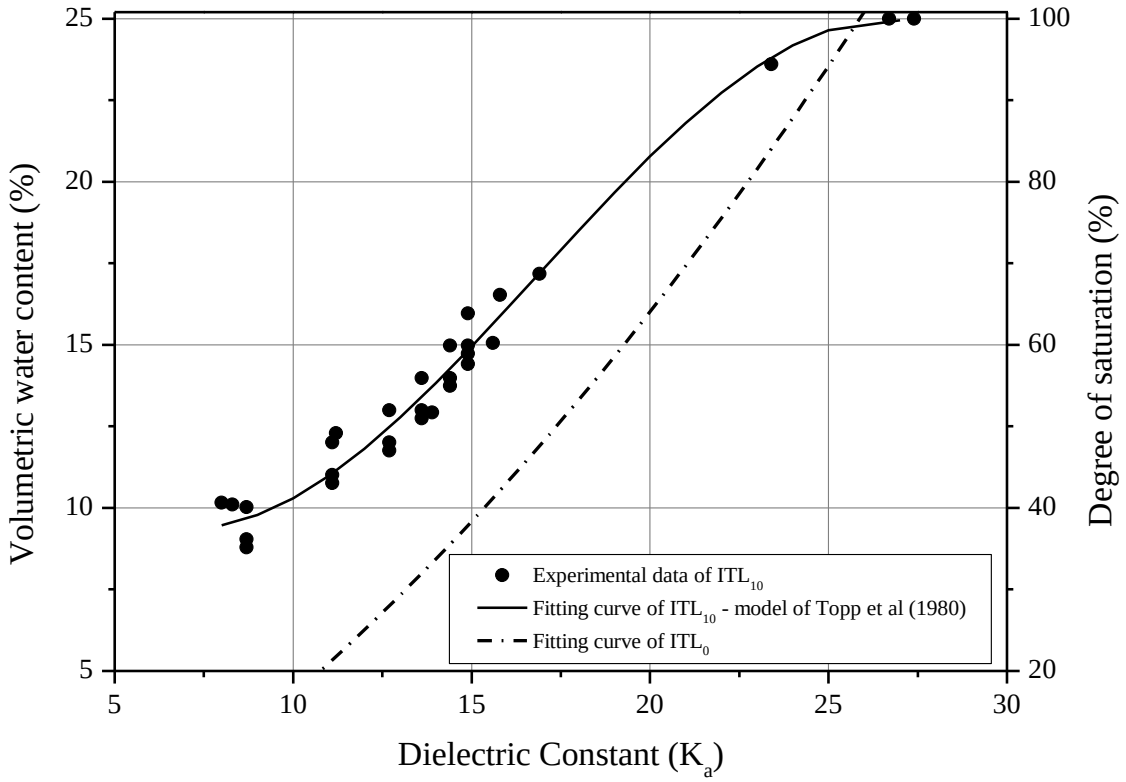
630

631 **Fig. 1: Grain size distribution curves of the interlayer soil (*ITL_0) and the derived ones* (*ITL_{10}* and *Fines*)**



632

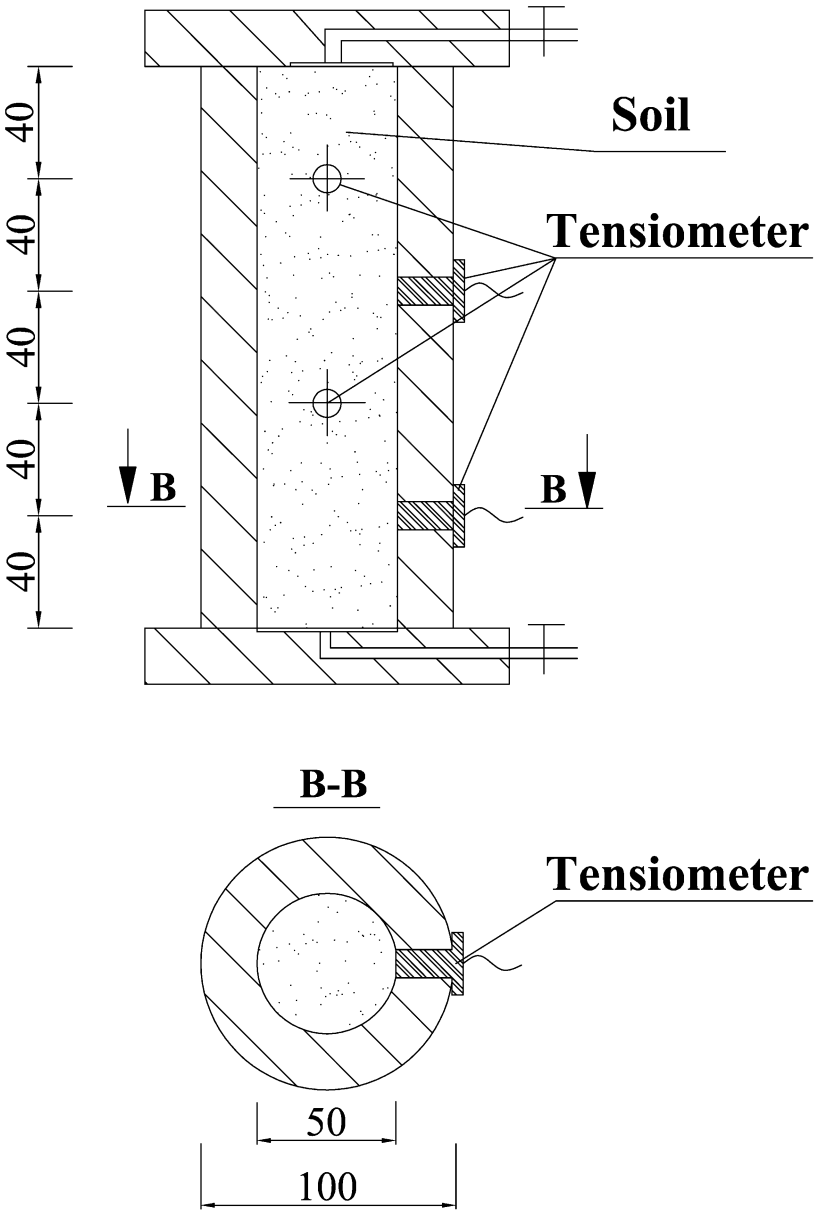
633 **Fig. 2: Schematic view of the large-scale infiltration column**



634

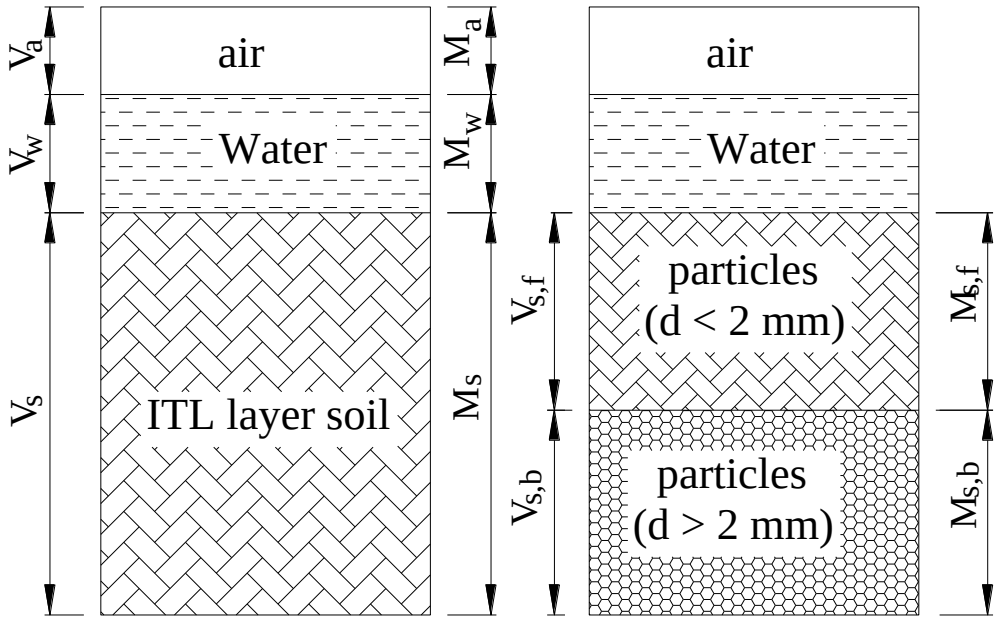
635 **Fig. 3: Calibration curves of the TDRs used for the *ITL$_{10}$* and *ITL$_0$* specimens**

636



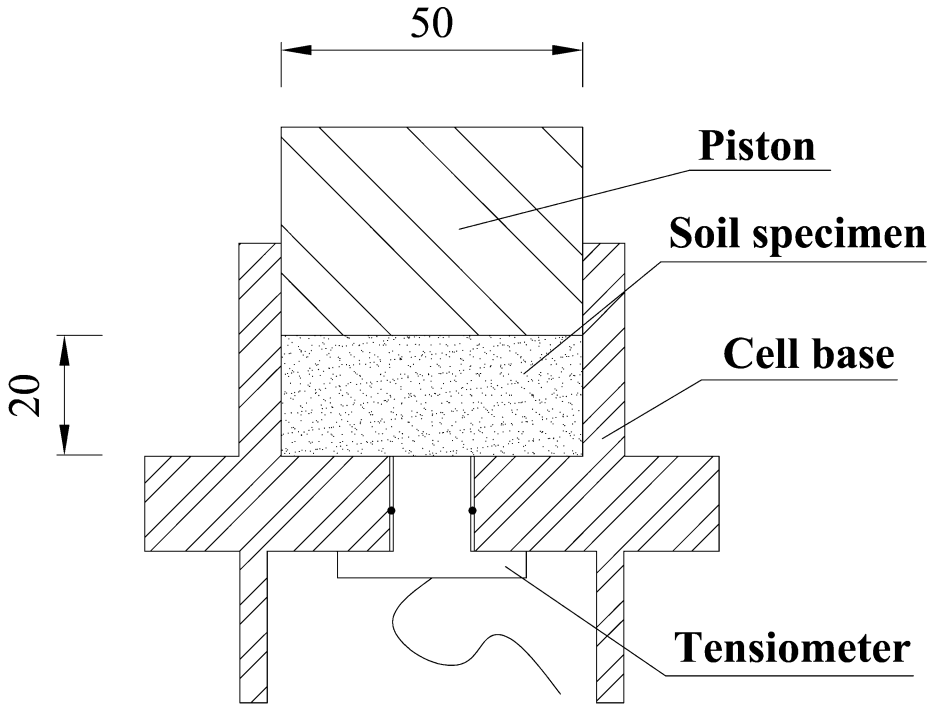
637

638 **Fig. 4: Schematic view of the small-scale infiltration column**



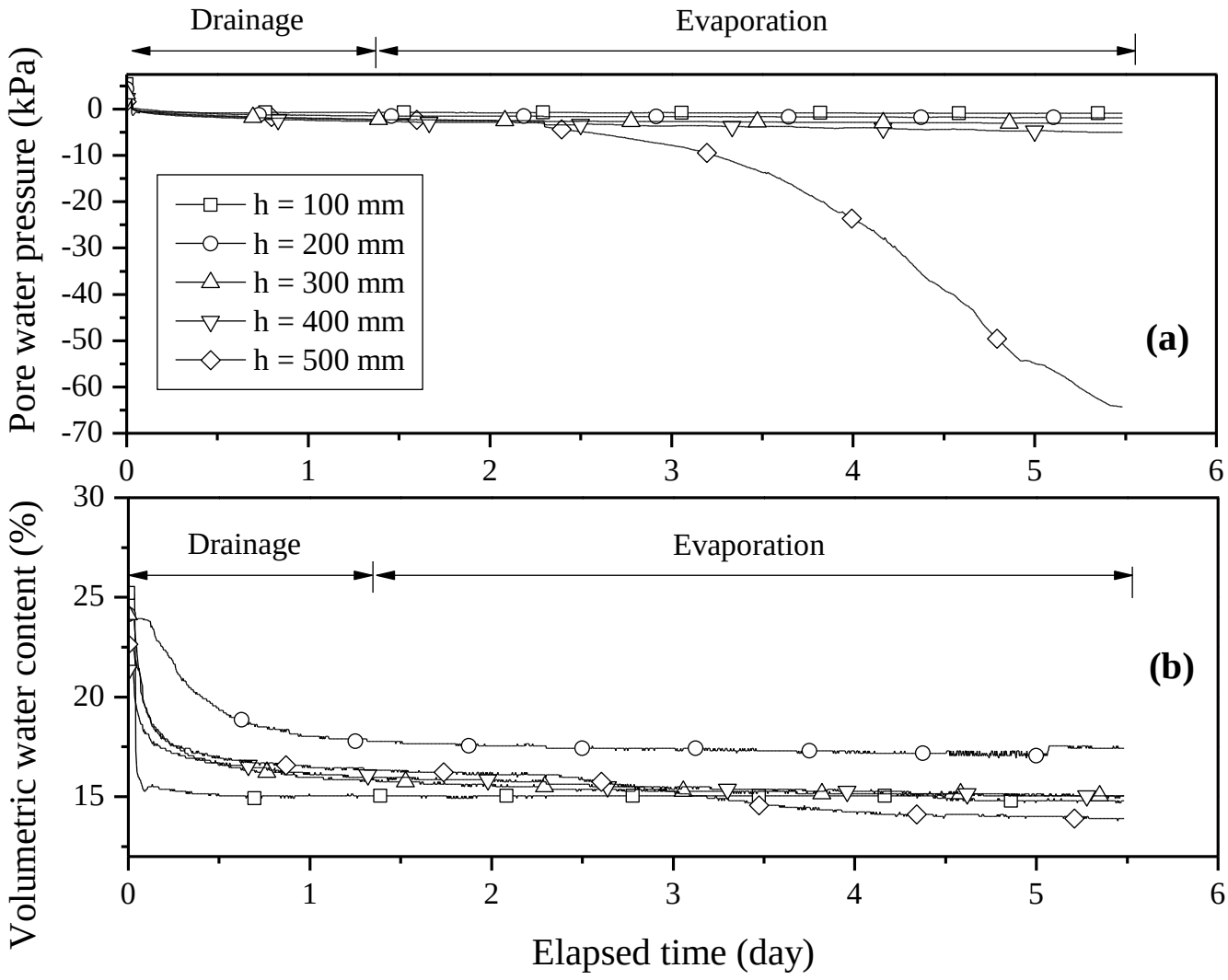
639

640 **Fig. 5: Components of the unsaturated interlayer soil**



641

642 **Fig. 6: Device for determining the WRC of** *Fines*



643

644 **Fig. 7: Test on ITL_{10}: pore water pressure and volumetric water content evolutions during Drainage 1 and**
645 **Evaporation 1**

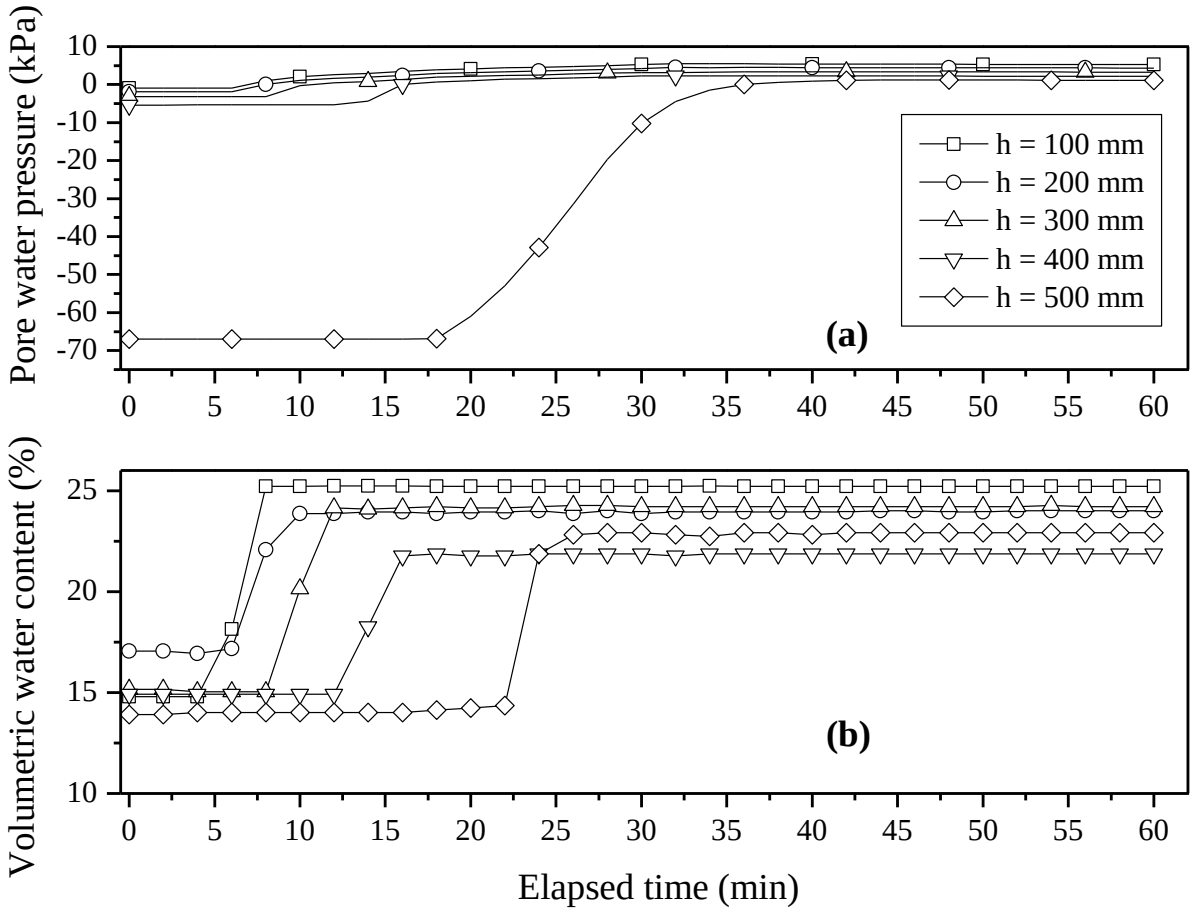
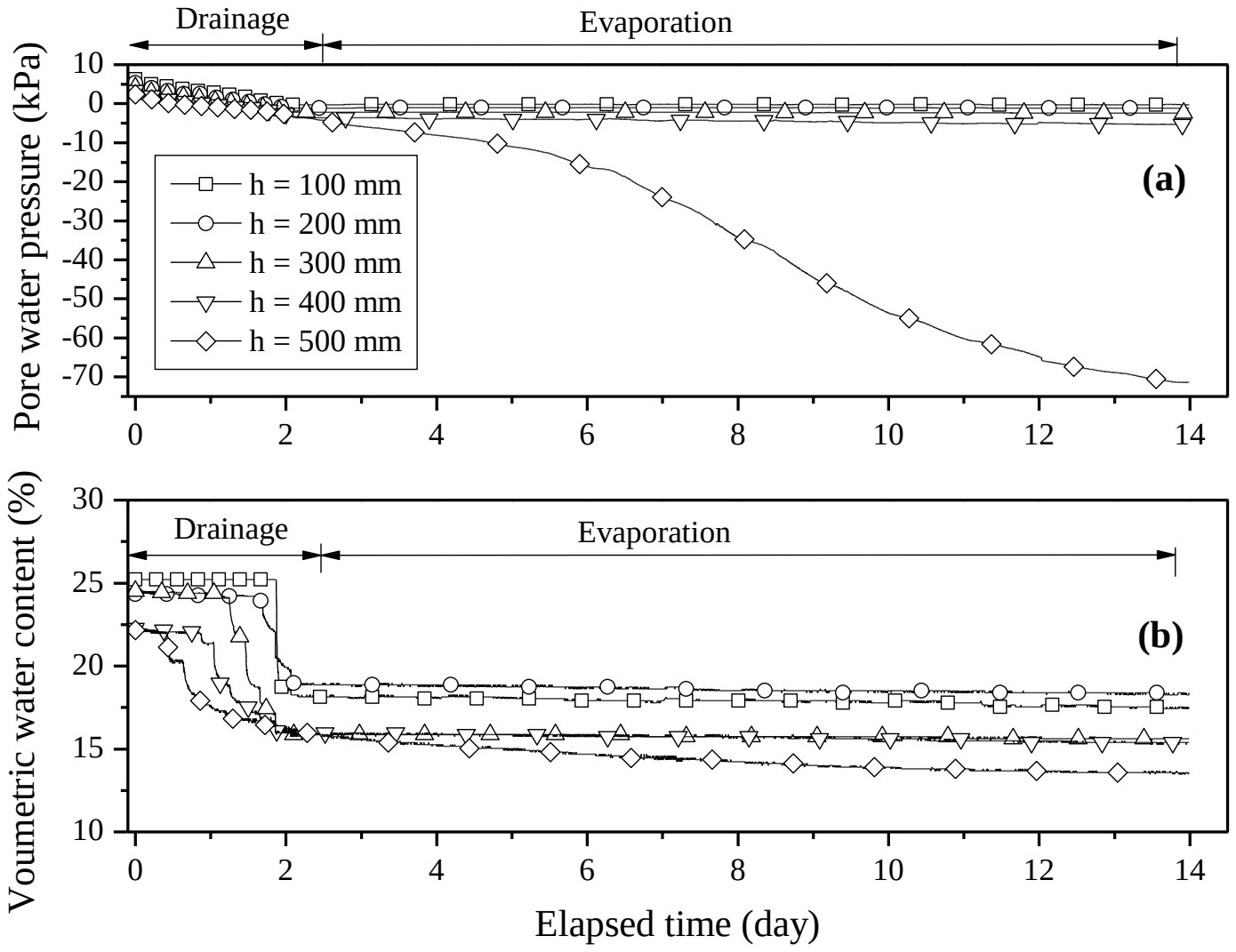
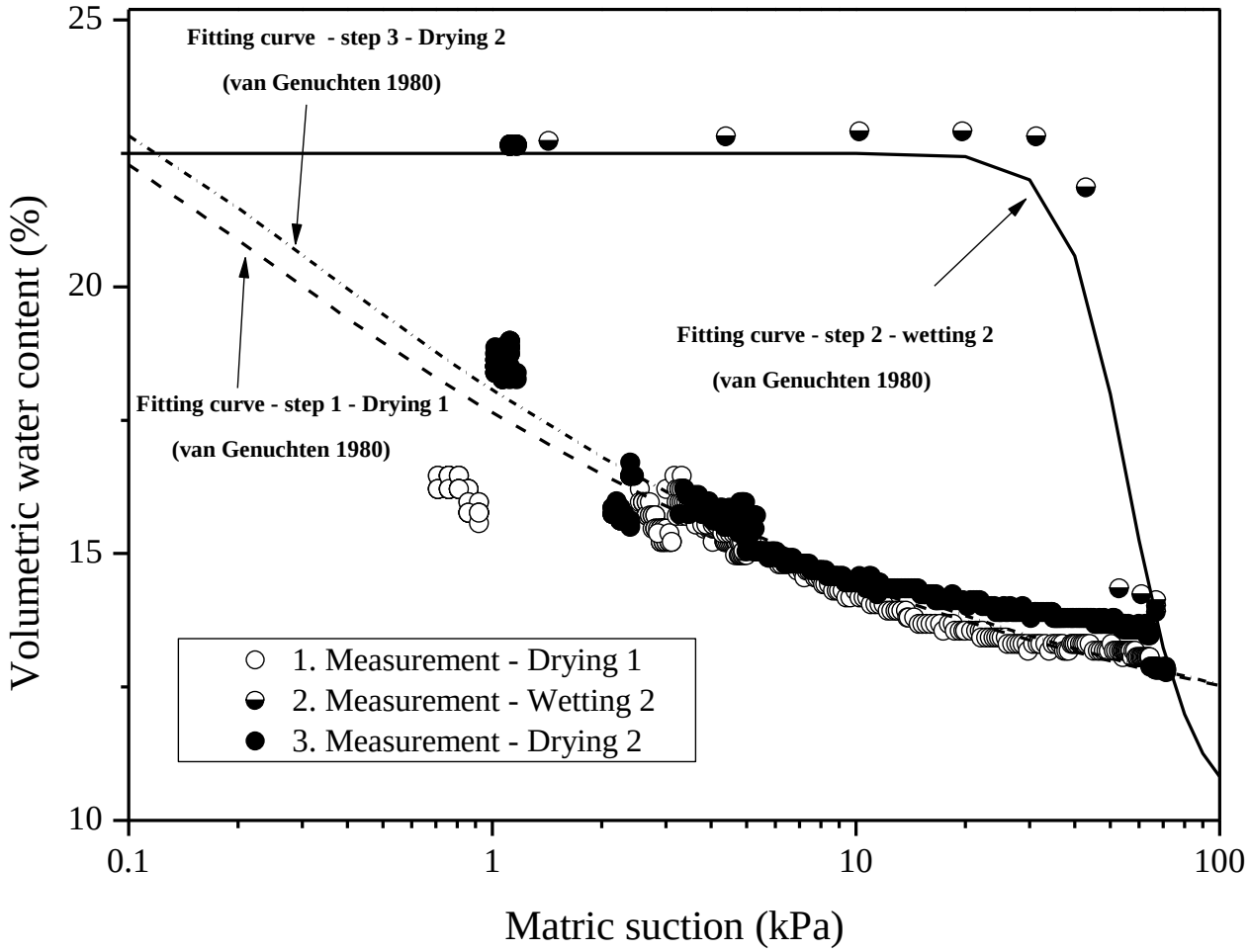


Fig. 8: Test on ITL_{10}: pore water pressure and volumetric water content evolutions in Saturation 2



649

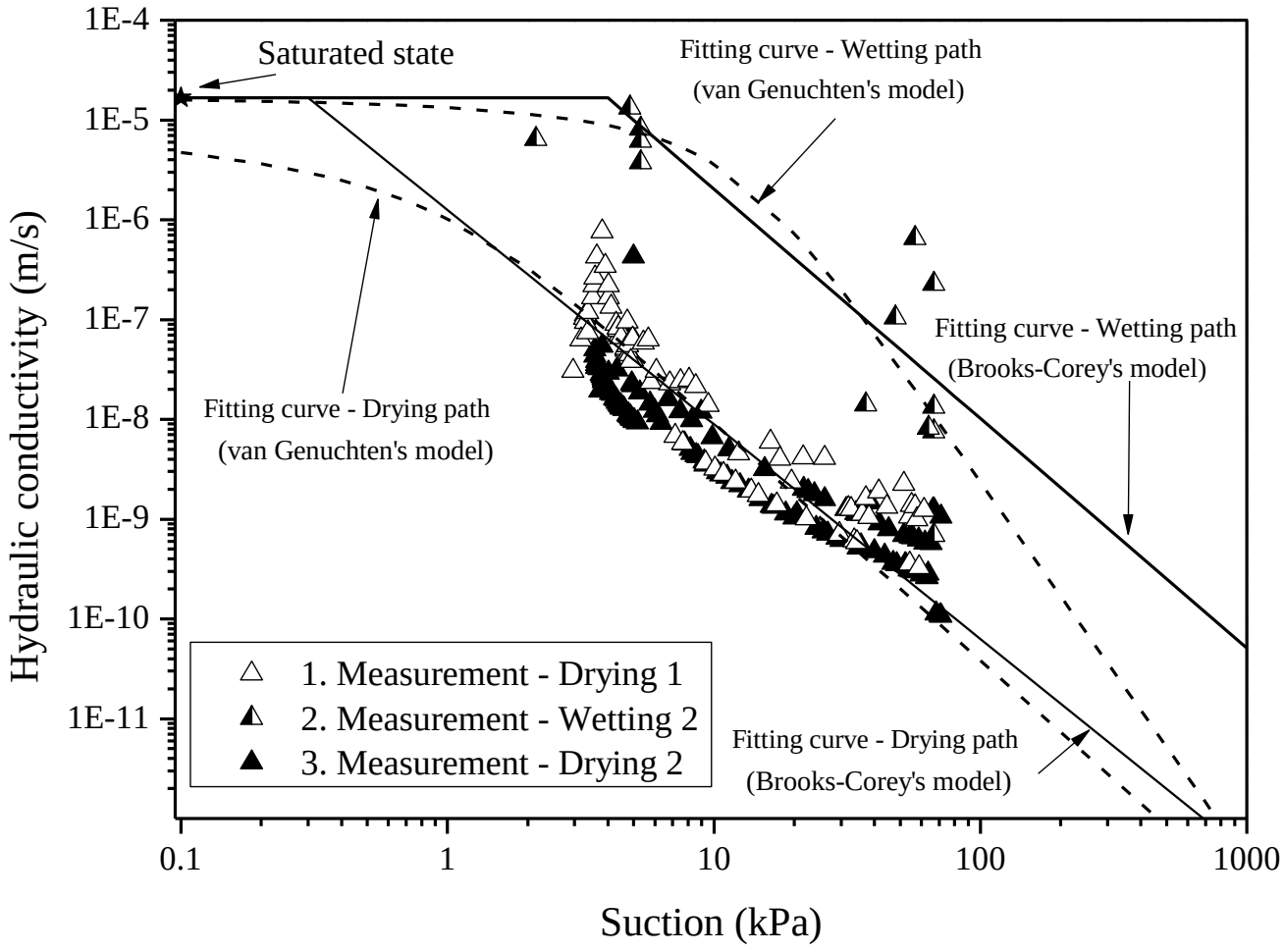
650 **Fig. 9: Test on ITL_{10}: pore water pressure and volumetric water content evolutions during Drainage 2 and**
651 **Evaporation 2**



652

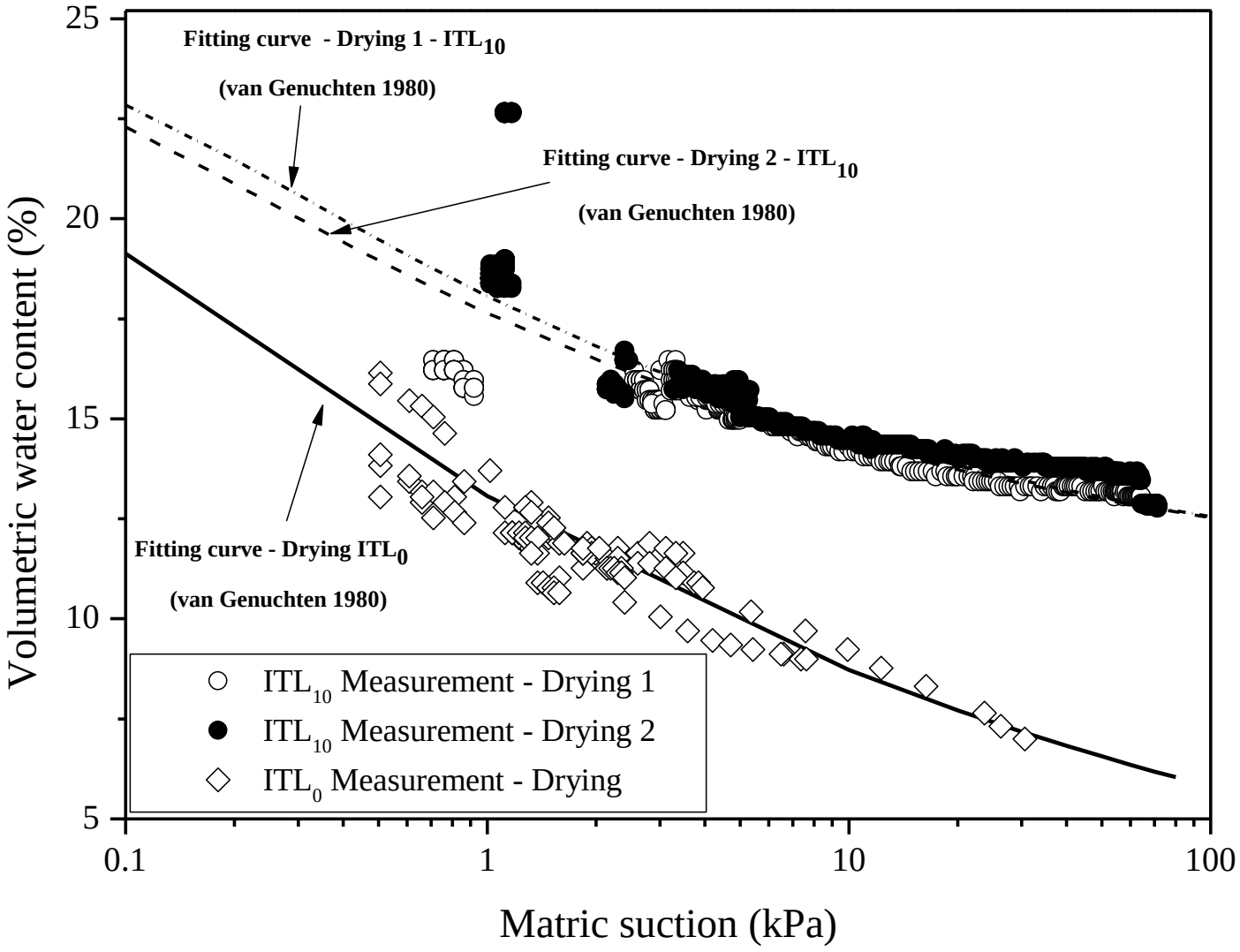
653 **Fig. 10: WRC of ITL_{10} with fitting curves using the van Genuchten's model (1980)**

654



655

656 **Fig. 11: Hydraulic conductivity of ITL_{10} obtained with drying-wetting cycles**

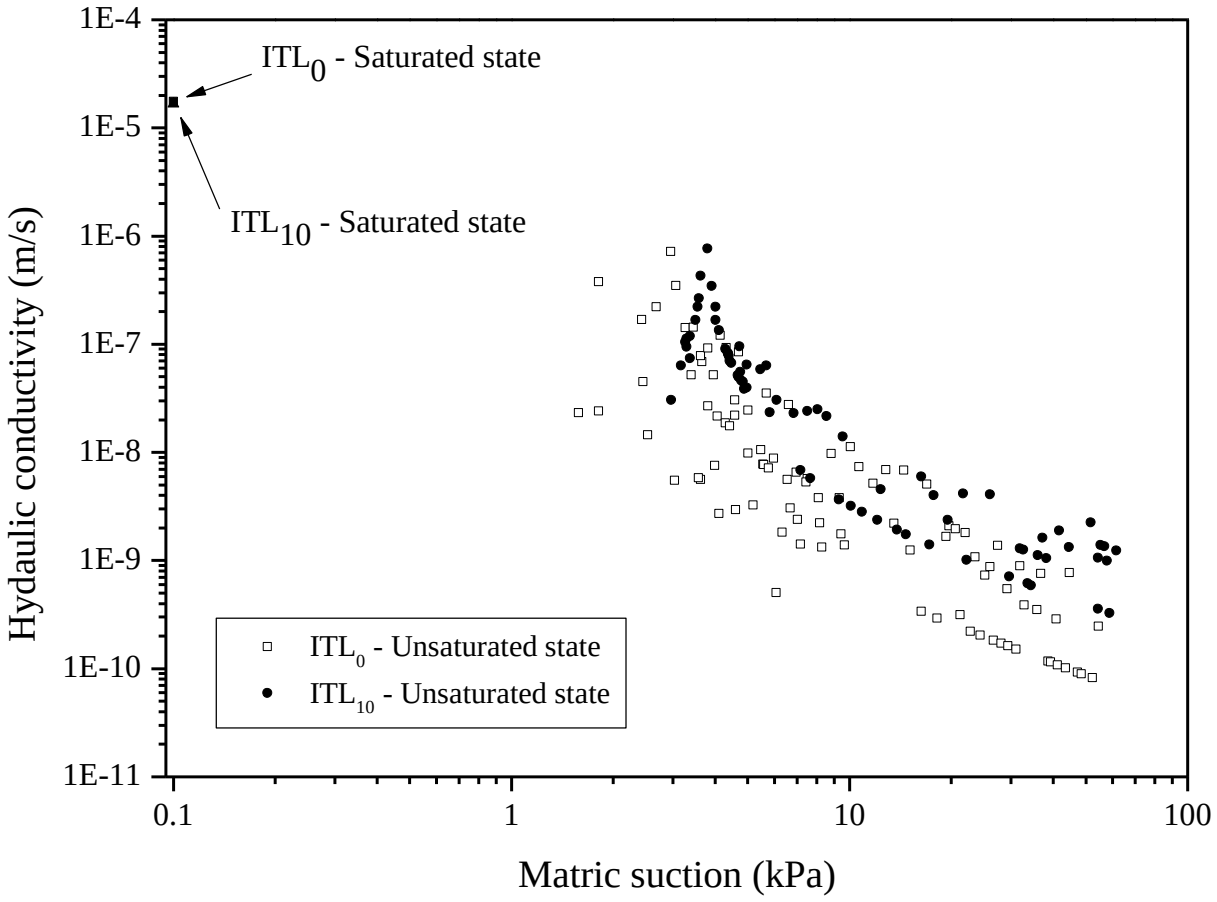


657

658 **Fig. 12: Comparison of SWRC between *ITL$_0$* and *ITL$_{10}$***

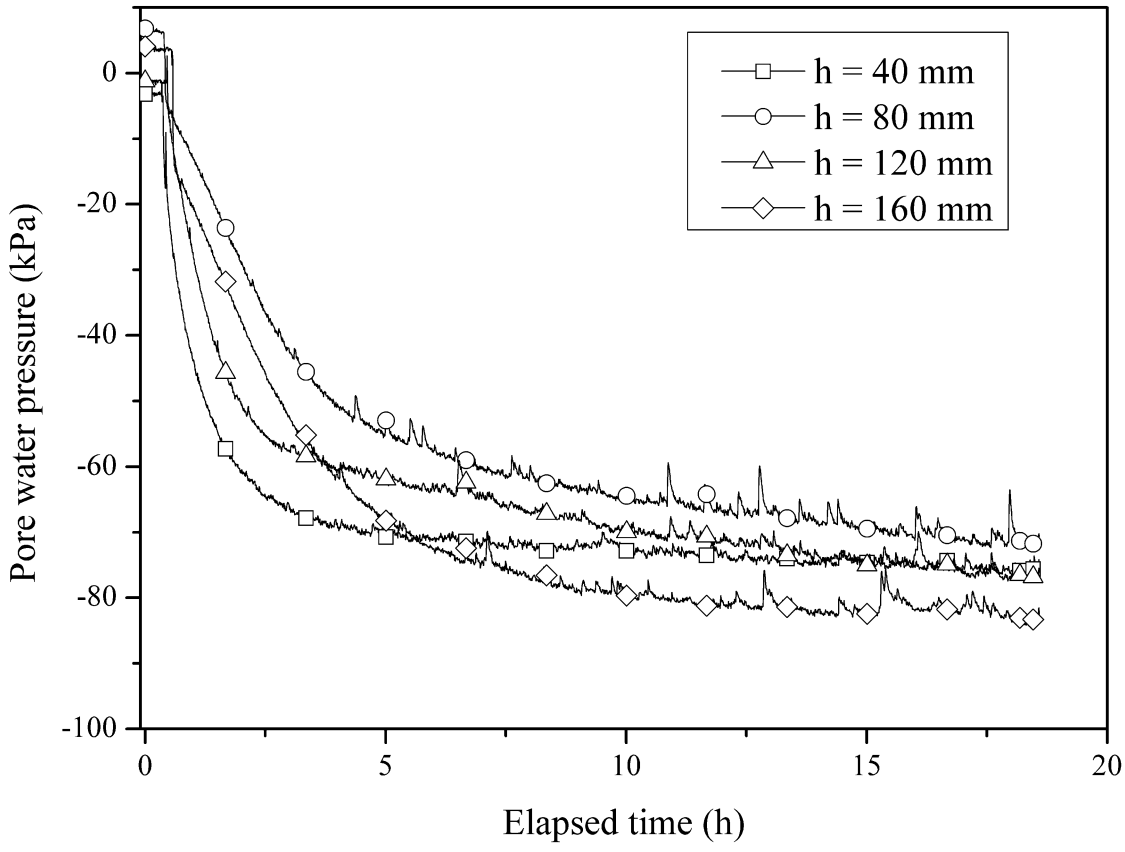
659

660



661

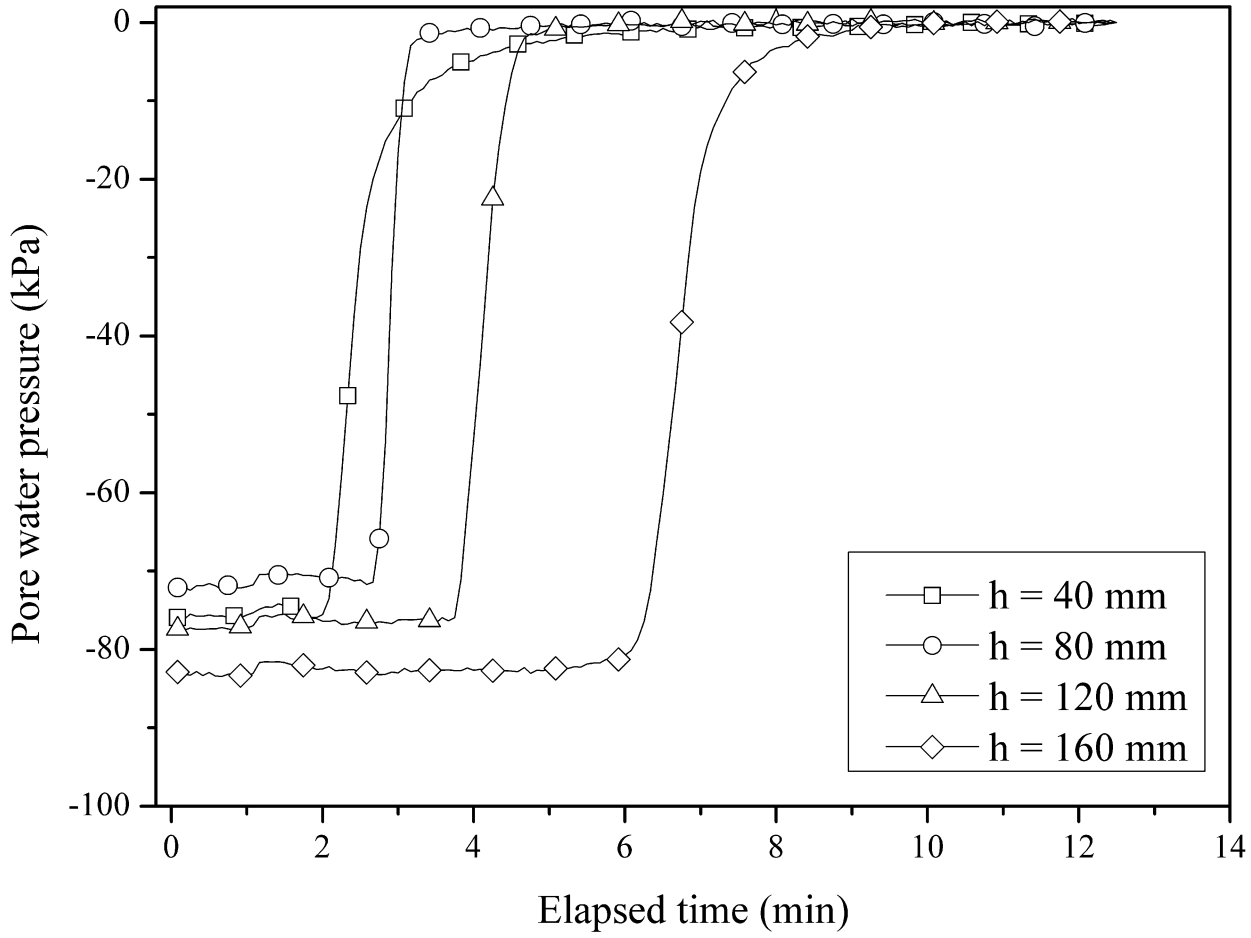
662 **Fig. 13: Comparison of hydraulic conductivity between *ITL$_0$* and *ITL$_{10}$***



663

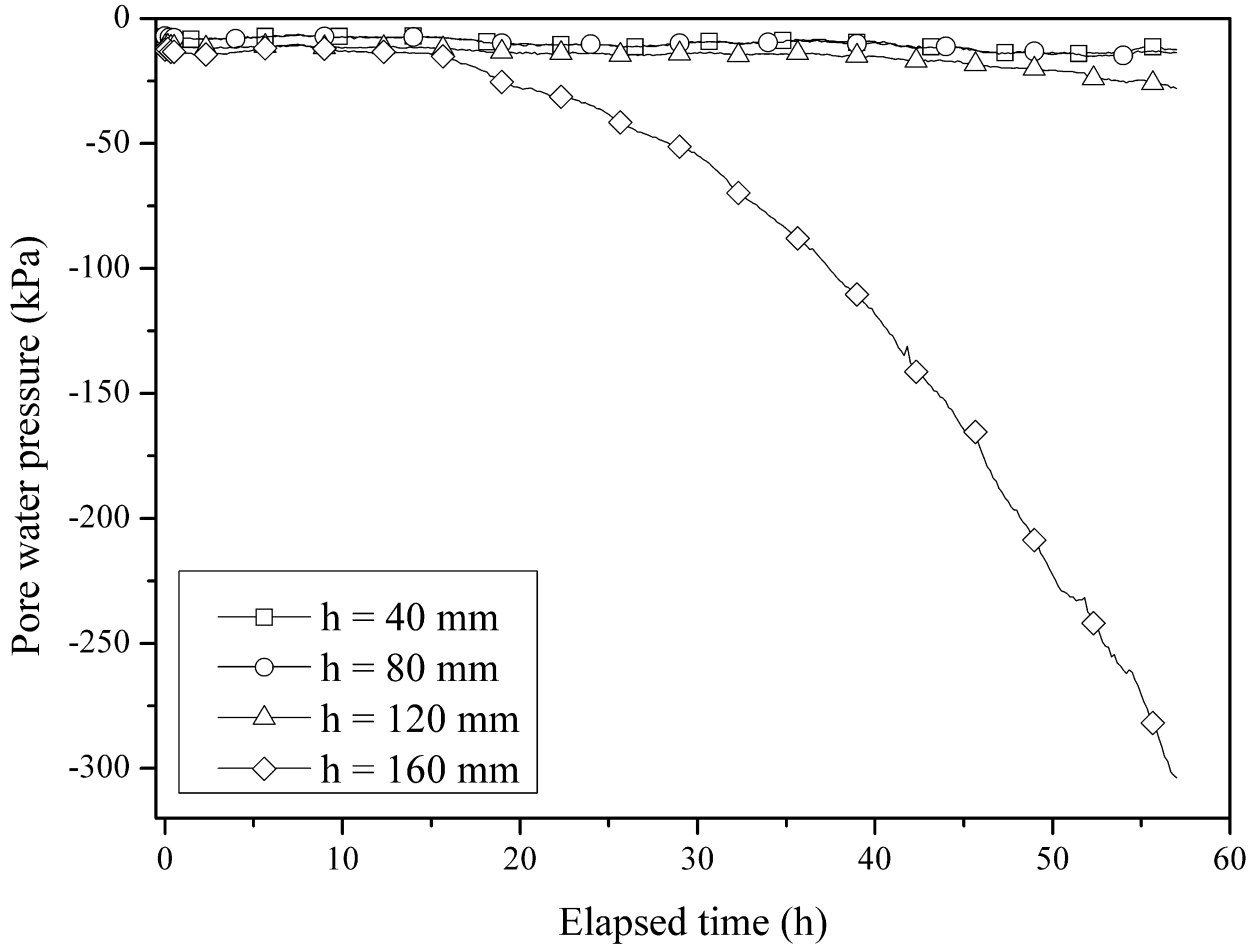
664 **Fig. 14: Test on *Fines*: suction stabilization after the installation of tensiometers**

665



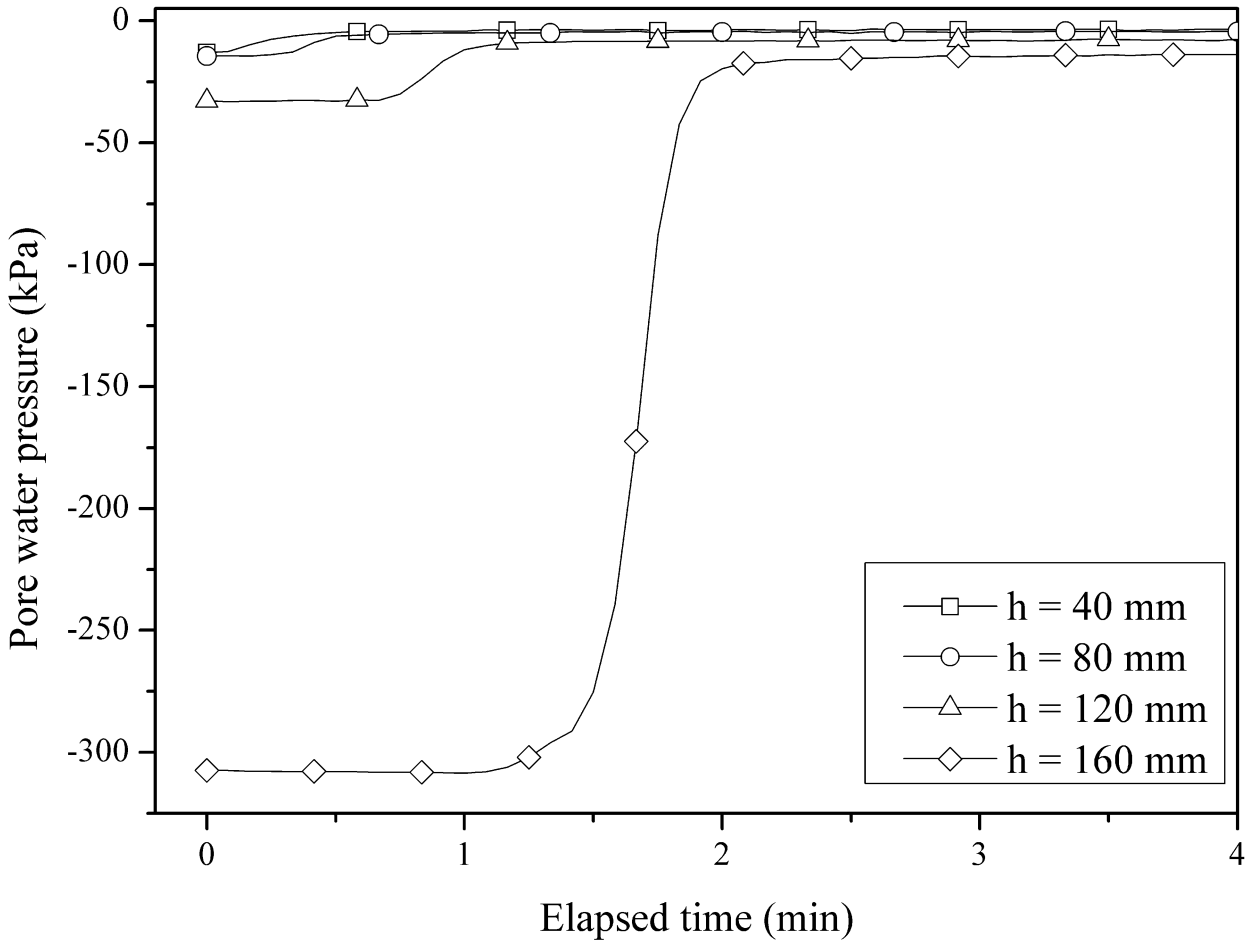
666

667 **Fig. 15: Test on *Fines*: suction evolutions during Saturation 1**



668

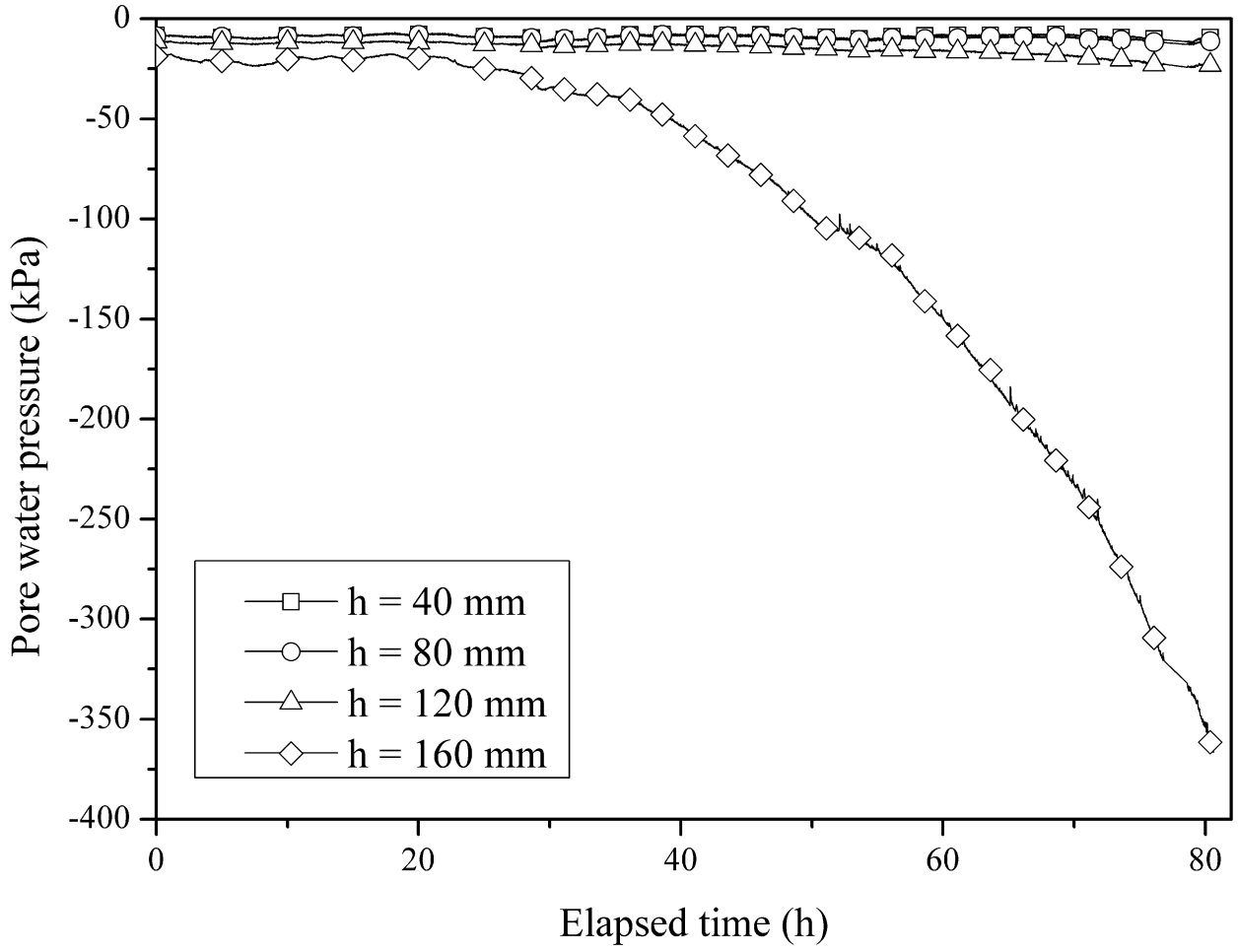
669 **Fig. 16: Test on *Fines*: suction evolutions during Evaporation 1**



670

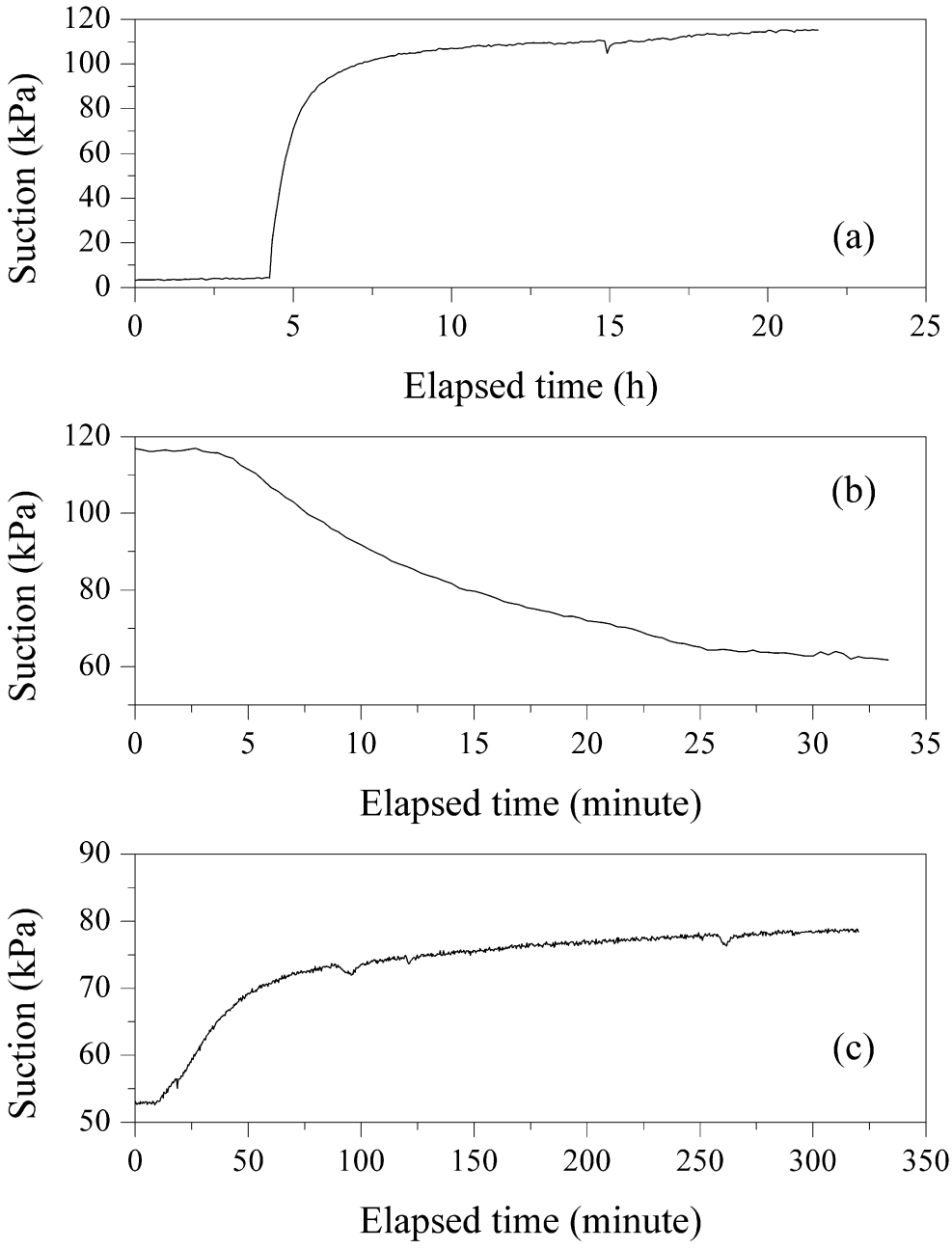
671 **Fig. 17: Test on *Fines*: suction evolutions during Saturation 2**

672



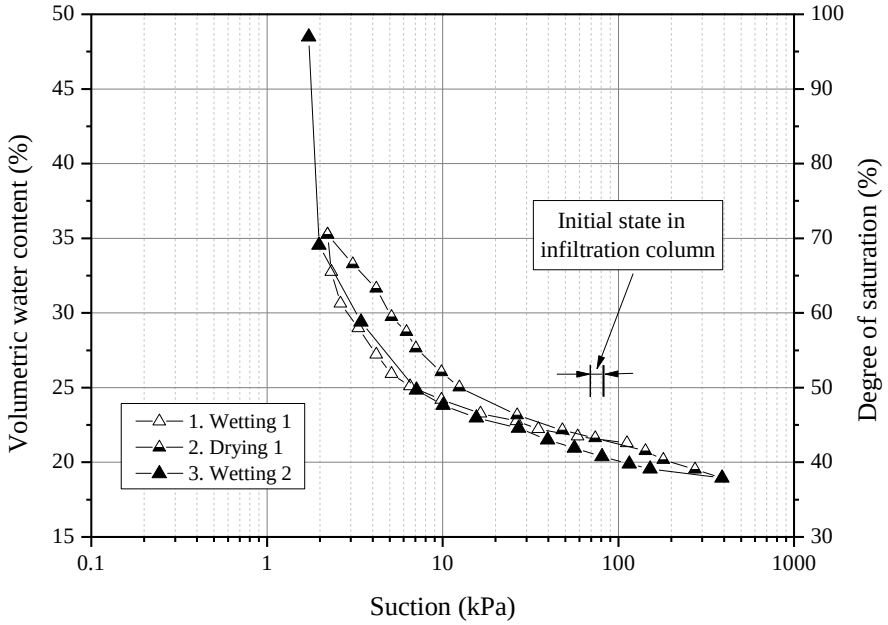
673

674 **Fig. 18: Test on *Fines*: suction evolutions during Evaporation 2**



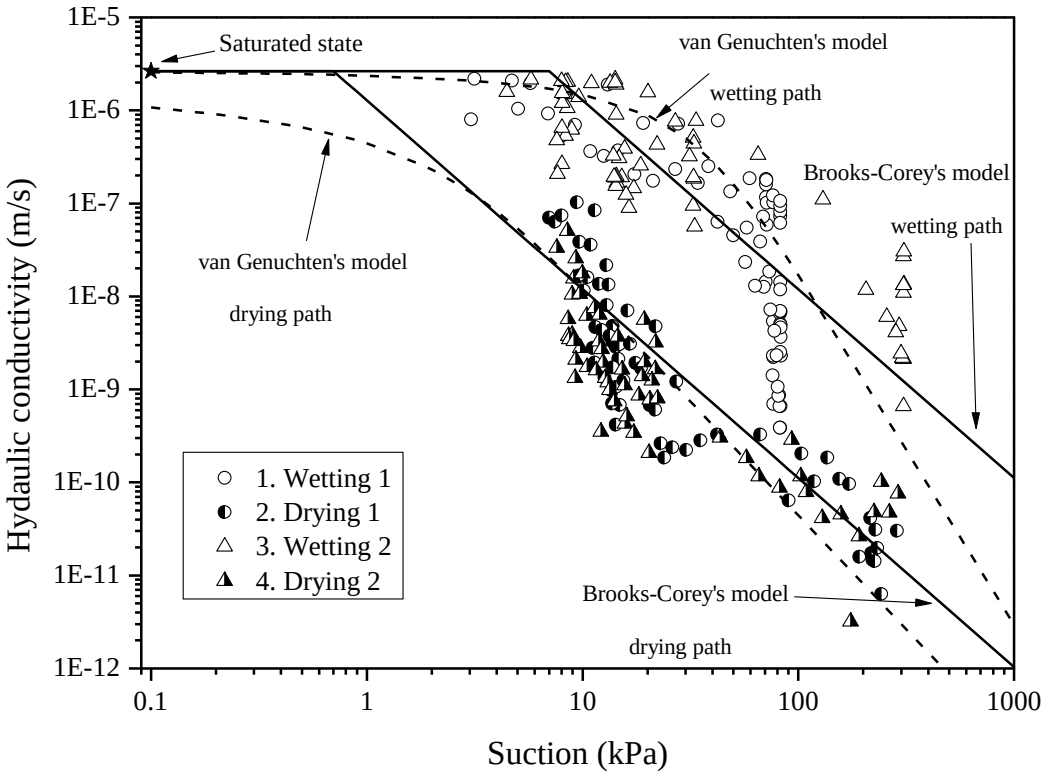
675

676 **Fig. 19: Stabilization of suction during the SWRC determination. (a) initial stabilization after tensiometer**
677 **installation, (b) a wetting stage, (c) a drying stage**



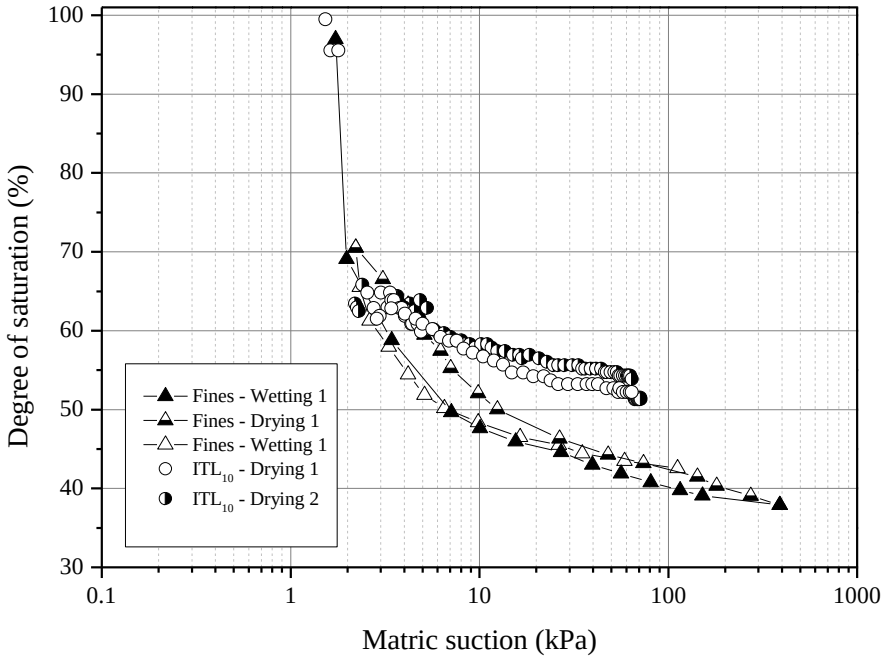
678

679 **Fig. 20: WRC of *Fines***



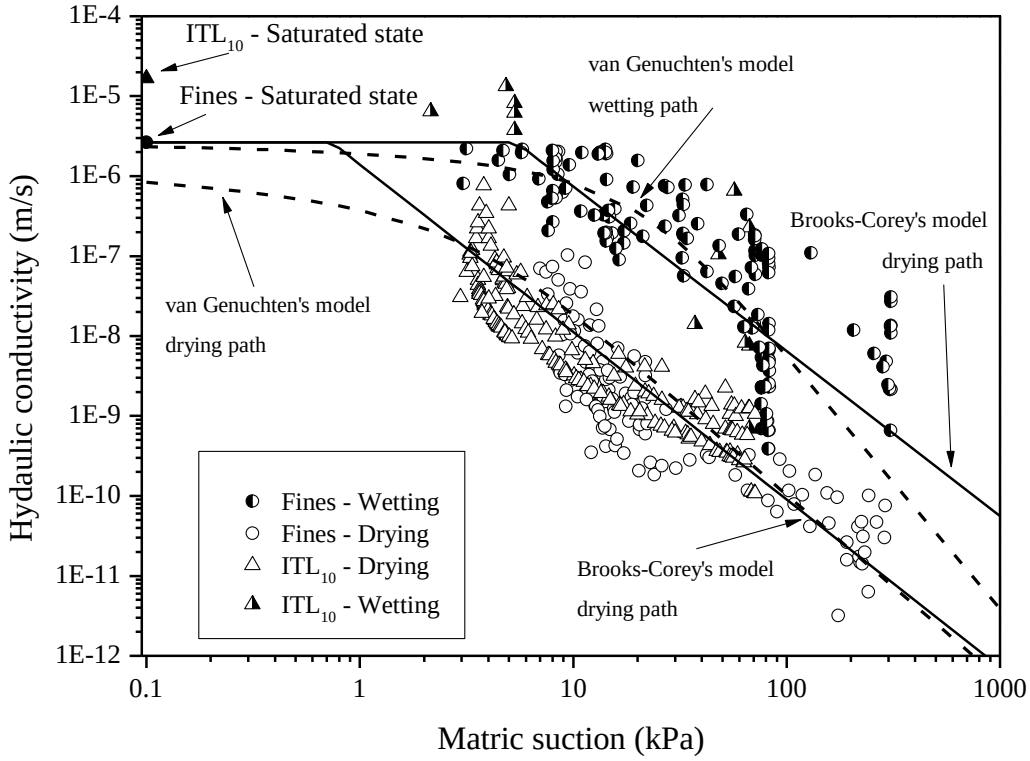
680

681 **Fig. 21: Hydraulic conductivity of *Fines*, obtained with drying/wetting cycles**



682

683 **Fig. 22: Comparison of SWRC between *ITL$_{10}$* and *Fines***



684

685 **Fig. 23: Comparison of hydraulic conductivity between *ITL$_{10}$* and *Fines***